https://ntrs.nasa.gov/search.jsp?R=19700027042 2020-03-11T23:33:18+00:00Z

CR-102820

TECHNICAL REPORT NO. 736

ANALYSES FOR THE DESCRIPTION OF ROCKET AND AIRBREATHING PROPULSION SYSTEM COMBUSTION CHAMBER AND NOZZLE FLOWS

By R. B. Edelman, O. F. Fortune, and G. Weilerstein

ANNUAL REPORT

Prepared Under Contract No. NAS8-21387

Prepared for

George C. Marshall Space Flight Center
Marshall Space Flight Center, Alabama 35812

April 1970

N70-36358
(ACCESSION NUMBER)
(THRU)
75
(PAGES)
1
(CODE)
CR-102820
(NASA CR OR TMX OR AD NUMBER)
28
(CATEGORY)
FACILITY FORM 602

RECEIVED
NASA STI FACILITY
INPUT BRANCH
SEP 1970

GENERAL APPLIED SCIENCE Labs., Inc.
MERRICK AND STEWART AVENUES, WESTBURY, L.I., NEW YORK 11590 • 516-333-6960
A SUBSIDIARY OF THE MARQUARDT CO

Reproduced by
NATIONAL TECHNICAL
INFORMATION SERVICE
Springfield, Va. 22151

N70-36358

ANALYSES FOR THE DESCRIPTION OF ROCKET AND AIRBREATHING PROPULSION SYSTEM COMBUSTION CHAMBER AND NOZZLE FLOWS

R.B. Edelman, et al.

April 1970

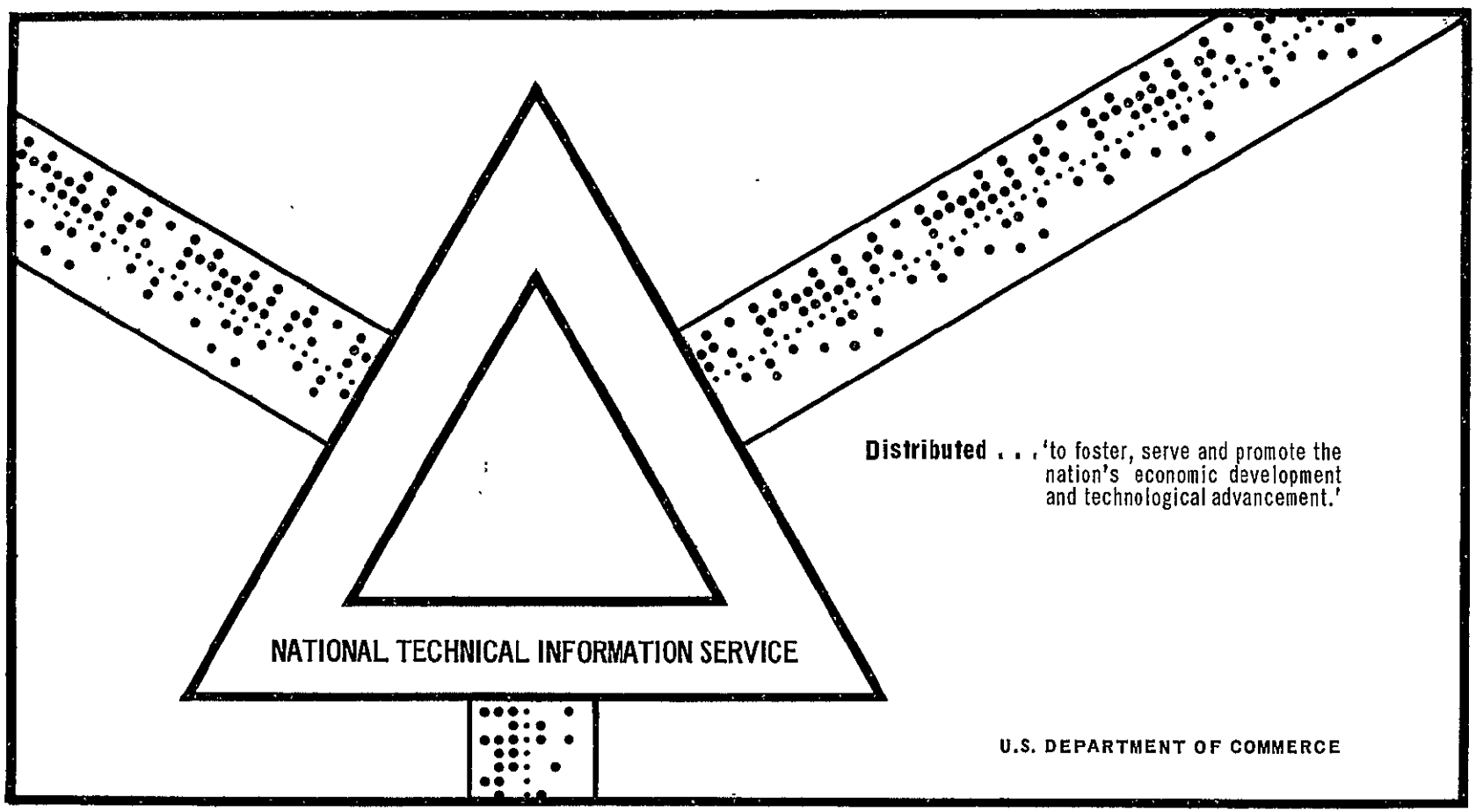

This document has been approved for public release and sale.

GASL TECHNICAL REPORT NO. 736

ANALYSES FOR THE DESCRIPTION OF ROCKET AND AIRBREATHING PROPULSION SYSTEM COMBUSTION CHAMBER AND NOZZLE FLOWS

By R. B. Edelman, O. F. Fortune, and G. Weilerstein

ANNUAL REPORT

Prepared Under Contract No. NAS8-21387

Prepared for

George C. Marshall Space Flight Center
Marshall Space Flight Center, Alabama 35812

Prepared by

General Applied Science Laboratories, Inc.
Subsidiary of The Marquardt Co.
Merrick and Stewart Aves.
Westbury, L.I., N.Y.

Approved by: L. M. Nucci
L. M. Nucci
President

April 1970

ABSTRACT

The work described in this report deals with analytical studies for the description of the coupled fluid mechanical and chemical kinetics processes occurring in rocket and air-breathing propulsion systems. The partial differential equations and numerical solution techniques for subsonic, supersonic and mixed flows are presented. Calculations, demonstrating the application of the analyses to combustion chamber and nozzle flow fields, are given.

TABLE OF CONTENTS

Section		Page No.
	Abstract	ii
I	Introduction	1
II	Analysis	3
	A. Parabolic Flows - The Liquid Propellant Rocket Combustion Chamber	3
	B. Hyperbolic and Mixed Hyperbolic/ Flows in Augmentation Chambers, Scramburners and Nozzles	18
III	Applications and Summary	25
	A. Applications	25
	B. Summary	27
	References	29
	Appendix A Input Formats for Parabolic Programs With Equilibrium and Quasi-Complete Combustion Models	31
	Appendix B Some Features of the Finite Difference Solution of the Parabolic Equations	41

LIST OF FIGURES

Figure No.		Page No.
1	Schematic of Propulsion Systems	46
2	Schematic of Rocket Motor Combustion Chamber Using Multiple Ring Injection Model	47
3	Comparison of Quasi-Complete Combustion Models with Equilibrium Chemistry for a Propane-Air System	48
4	Comparison of Quasi-Complete Combustion Models with Equilibrium Chemistry for a Propane-Air System	49
5	Early Quasi-Complete Combustion of Hydrocarbon-Air Chemistry Model (Model A)	50
6	Final Quasi-Complete Combustion Hydrocarbon-Air Chemistry Model (Model B)	51
7	Schematic of Mixed Flow Concept	52
8	Intrinsic Coordinate System	53
9	Computation Procedure	54
10	Procedure for Matching Along Separating Streamline	55
11	Profiles of Pressure, Mach Number, and Flow Angle at Initial Station	56
12	Axial Variations in Pressure, Temperature, Density, and Velocity for Subsonic Region	57
13	Computed Area Variation of Subsonic Region	58
14	Scale Drawing of Cornell Lab Ethylene-Oxygen Rocket Engine	59
15	Axial Static Pressure Comparison	60
16	Velocity Profile Comparison	61
17	Temperature Profile Comparison	62
18	Oxygen Equivalence Ratio Profile Comparison	63
19a	Wall	64
19b	Wall	65

LIST OF FIGURES (contd)

20a	Centerline	66
20b	Centerline	67
21	End Station	68

NOMENCLATURE

c_f	skin friction coefficient
h	static enthalpy
H	total enthalpy
Le	Lewis number
n	coordinate measured normal to the streamline
p	static pressure
Pr	Prandtl number
q	total velocity
r	radial coordinate
r_L	particle radius
s	coordinate measured along streamline
Sc	Schmidt number
T	static temperature
u	streamwise component of velocity
$\dot{w}_i$	production rate of the ith species
x	streamwise coordinate
y	lateral or radial coordinate
α^i	i^{th} species
$\tilde{\alpha}^j$	j^{th} element mass fraction
ϵ	characteristic angle relative to the streamline direction
$\epsilon_{p,g}$	diffusivity of particles and gas, respectively
μ_t	mixture viscosity

μ_{ty}	gas phase viscosity
θ	flow direction relative to axial coordinate
ρ	density
τ	$\equiv \tan \theta$
τ_w	wall shear
φ	equivalence ratio
ψ	stream function

<u>Subscripts</u>

pc	potential core
DSL	separating streamline
n,M	generic point in the x, ψ finite difference grid

I. INTRODUCTION

The existing tools for analysis of propulsion system components and overall performance characteristics involve, to a large degree, the application of one-dimensional concepts (References 1 and 2). Such treatments are essential in determining the potential performance of a given system and to a certain extent, provide an assessment of the apparent importance of some of the relevant processes which when coupled constitute the complex aerothermodynamic problem of detailed propulsion system analysis.

In general the flows of interest involve a number of coupled processes, including homogeneous chemical reactions, phase transition, and mixing within and between the phases. One principle limitation of the tools referred to above is the lack of coupling between these phenomenon. In addition, their treatment of the combustion process is limited and as a result some of the important mechanistic detail is lost. The limitations of the current capability as gaged by the status of the ICRPG programs for rocket motor analysis has been recently summarized in Reference 3 .

In particular, that article states:

"The following desirable improvements in calculation capability would increase the scope of applicability and the accuracy:

1) A physically realistic combustion(ηER) model which relates the multiple stream tube generation of product gases in the finite combustion chamber to the injected propellant mass flux and droplet size distributions.

2) An expanded list of chemical elements and compounds which can be handled.

3) Consideration of the effects of solid particles (as well as liquid droplets) in the combustion chamber.

4) Consideration of the effect of mixing along stream tube boundaries.

5) Refinement of the nozzle convergent region treatment to include: a) two-dimensional flow, b) kinetic effects, c) solid particles and liquid droplets in flow, d) continuing evaporation and chemical reaction with gas generation and heat release in this region, and e) multiple stream tubes.

6) Refinement of the transonic nozzle analysis to handle, a) small throat curvature ratios, b) multiple stream tubes (discontinuous sonic surface), c) liquid droplets, evaporation, and continuing reaction, d) kinetics, and e) solid particles in the flow.

7) Inclusion of the effects of, a) multiple stream tubes, b) liquid droplets, evaporation, and continuing reaction, d) kinetics, and e) solid particles in the flow.

8) Modification of the boundary-layer treatment to account for geometry effects on its development.

9) Acquisition of additional and more precise physical data, and a) droplet size and mass distribution resulting from injection processes, b) droplet shattering and evaporation in a hot gas stream, c) chemical reaction rates, and d) multistream tube mixing rates."

The present effort includes airbreathing as well as rocket motor analysis and addresses itself to the bulk of the above problems.

The chief purpose of the present work is to expand the computational framework for the analysis of flows which can treat the many simultaneous and coupled processes in airbreathing and rocket type propulsion systems.

The work presented in this annual report covers combustor and nozzle flow fields, including combustion, phase transition and mixing.

II. ANALYSIS

The propulsion systems of interest here cover a wide spectrum of combustion chamber flow regimes, ranging from relatively low speed rocket combustion chambers to high speed scramburners. Included within these limits are families of composite engines such as ducted and shrouded rockets, ejector ramjets, and so on. The composite concept is attractive for applications requiring low speed take-off and climb, and then efficient operation in the hypersonic flight regime. The elements of the various propulsion systems are shown schematically in Figure 1.

Common to each of the engine concepts is the coupling of mixing and combustion as the fuel and oxidizer are brought into contact. However, depending upon the characteristic scales of the flow and the relative importance of inertia compared with viscous effects, the pressure field can become a crucial additional consideration in the flow field analysis. Thus, in a rocket combustion chamber where the velocities are subsonic only "streamwise" pressure gradients will be of potential importance. However, in augmentation chambers involving mixed subsonic/supersonic flows, in scramburners, and nozzles, both "streamwise" and "lateral" pressure variations can be important.

The analyses which are described here are designed to treat the spectrum of such flows.

A. Parabolic Flows - The Liquid Propellant Rocket Combustion Chamber

A schematic of this type of flow field is shown in Figure 2. In general, the processes which occur in the immediate neighborhood of the injector face are very complex, and are not yet well defined analytically. This is in part due to the multiplicity of injection configurations which are in use, such as

elements comprised of single jets (showerhead), impinging streams (like or unlike doublets, triplets, etc.), concentric tubes, impinging sheets and swirl cup injectors. Nevertheless, for certain of the geometries an approximate model involving a "concentric ring" representation, as shown in Figure 2, is appropriate. Such a model provides a rationale for establishing initial conditions and is a geometric simplification in that the flow may be treated as an axisymmetric flow throughout the entire chamber.

In previous work[4,5] the problem of describing and numerically solving an axisymmetric, or plane two-dimensional, ducted flow field using the parabolic boundary layer conservation equations has been treated. Also, a finite-rate chemistry model was developed to describe the high temperature combustion of air and JP or RP fuels (of References 6 , 7 , and 8), and was coupled to a mixing analyses. For purposes of engine design and/or performance analysis, experience has shown that the most practical procedure is to make calculations over a wide range of conditions, using chemically frozen or chemical equilibrium models, and then use the finite rate chemical kinetics model for those conditions which have proved to be of the greatest interest. Hence it was necessary to develop a reliable hydrocarbon-air equilibrium chemistry model and couple it to a suitable ducted mixing analysis. In the course of this work, it was found that it was possible to formulate relatively simple "quasi-complete combustion" chemistry models which accurately reproduced the thermodynamic equilibrium models in terms of flame temperature (for temperatures up to 2500°K, where dissociative affects first become significant), and which included solid carbon as a specie

for highly fuel-rich stoichiometric ratios. This makes it possible to perform equilibrium-like calculations for little more than the cost of a chemically frozen calculation, and reserve the more expensive thermodynamic equilibrium model, along with the quasi-global finite rate model for the most important sets of operating conditions.

The flow field conservation equations for the ducted problem, with equilibrium chemistry, are presented below.

The analysis includes the capability for treating phase transition effects appropriate to liquid fueled motors. In fact, for generality both evaporation and condensation are included in the analysis using classical nucleation and growth theory as detailed in Ref. 9. The computer program was developed considering CO_2 or H_2O as species which may appear in two phases but the analysis may be readily extended to include other species such as the fuel and oxidizer.

Referring to Figure 2, the describing equations in Von Mises coordinates for the ducted mixing and combustion process are given by:

Momentum:

$$\frac{\partial u}{\partial x} = -\frac{1}{\rho u}\frac{dp}{dx} + \frac{1}{\psi^N}\frac{\partial}{\partial \psi}\left(a\frac{\partial u}{\partial \psi}\right)$$

Energy:

$$\frac{\partial H}{\partial x} = \frac{1}{\psi^N}\frac{\partial}{\partial x}\left(a\left[\frac{1}{Pr}\frac{\partial H}{\partial \psi} + \left(1-\frac{1}{Pr}\right)\frac{\partial\left(\frac{u^2}{2}\right)}{\partial \psi} + \sum_i\left(\frac{1}{Sc}-\frac{1}{Pr}\right)h^i\frac{\partial \alpha^i}{\partial \psi}\right]\right)$$

Species Diffusion:

Elements:

$$\frac{\partial \tilde{\alpha}^j}{\partial x} = \frac{1}{\psi^N} \frac{\partial}{\partial \psi}\left(\frac{a}{Sc} \frac{\partial \tilde{\alpha}^j}{\partial \psi}\right) + \frac{\tilde{\dot{w}}_L^j}{\rho u}$$

Phase Transition Specie:

$$\frac{\partial \alpha_L}{\partial x} = \frac{1}{\psi^N} \frac{\partial}{\partial \psi} \left(\frac{a}{Sc} \frac{\partial \alpha_L}{\partial \psi}\right) + \frac{\dot{w}_L}{\rho u}$$

The transformation employed in arriving at the above equations is given by:

$$\psi^N \psi_y = \rho u y^N$$

$$\psi^N \psi_x = -\rho v y^N$$

where the stream function, ψ identically satisfies the continuity equation, and

$$a \equiv \frac{\mu \rho u y^{2N}}{\psi^N}$$

Furthermore,

$$\alpha_L + \sum_{j=1}^{\text{elements}} \tilde{\alpha}_j = 1$$

$$\tilde{\alpha}^j = \sum_{i,j} \nu_{i,j} \frac{W_j}{W_i} \alpha^i \; ; \quad \tilde{\dot{w}}^j = \sum_{i,j} \nu_{L,j} \frac{W_j}{W_L} \dot{w}_L$$

where

$$N = \begin{cases} 0 \text{ for plane two-dimensional flow} \\ 1 \text{ for axisymmetric flow} \end{cases}$$

and $\nu_{i,j}$ is the stoichiometric coefficient of element j in specie i.

Finally, the ideal gas law is used for the equation of state:

$$p = \rho R_o T \sum^{\text{all gas}} \frac{\alpha^j}{w^j}$$

Boundary Conditions

$$\text{at} \quad \psi=0; \quad \frac{\partial u}{\partial \psi} = \frac{\partial \alpha^k}{\partial \psi} = \frac{\partial H}{\partial \psi} = 0$$

$$\text{at } \psi=\psi_w \quad \begin{aligned} \frac{\partial u}{\partial \psi} &= \left(\frac{\psi}{\rho u y}\right)_w \left(\frac{\rho u^2}{\mu}\right)_{BULK} \frac{C_f}{2} \\ &= \left(\frac{\psi}{\rho u y}\right)_w \frac{\tau_w}{\mu t} \\ \frac{\partial H}{\partial \psi} &= 0, \text{ or } T = T_w \\ \frac{\partial \tilde{\alpha}^k}{\partial \psi} &= 0 \end{aligned}$$

Initial Conditions

$$x = 0 \qquad 0 \le \psi \le \psi_1 \qquad \begin{cases} u = u_1(\psi) \\ H = H_1(\psi) \\ \tilde{\alpha}^K = \tilde{\alpha}_1^k(\psi) \\ \alpha_L = \alpha_{L1}(\psi), \text{up to } 10 \\ r_L = r_{L1}(\psi), \text{up to } 10 \end{cases}$$

$$\psi_1 < \psi \le \psi_2 \qquad \begin{cases} u = u_2(\psi) \\ H = H_2(\psi) \\ \tilde{\alpha}^k = \tilde{\alpha}_2^k(\psi) \\ \alpha_L = \alpha_{L_2}(\psi) \\ r_L = r_{L_2}(\psi) \end{cases}$$

$$\psi_i < \psi \le \psi_w \qquad \begin{cases} u = u_i(\psi) \\ H = H_i(\psi) \\ \tilde{\alpha}^k = \tilde{\alpha}_i^k(\psi) \\ \alpha_L = \alpha_{L_i}(\psi) \\ r_L = r_{L_i}(\psi) \end{cases}$$

In the above analysis, ten classes of particles are provided for. The classes are defined initially by fixing the size range of each class. This criterion applies to all the annuli at the initial station, and for all subsequent stations which are computed during the development of the flow field.

The boundary conditions currently employed incorporate the assumption of no mass transfer through the wall and symmetry of the flow field about the centerline. However, provision is made to account for wall drag and heat transfer. In certain flows the wall boundary layer will influence only a small part of the bulk flow and a detailed wall boundary layer treatment is not required. An examination of some relevant experimental data, Reference 10 (velocity profiles across the duct), shows that the details of the wall boundary layer are not a dominant influence on the development of the bulk flow field. Thus, in the present analysis the gross effects of the wall boundary layer are included without resorting to detail. Hence, instead of specifying $u = 0$, the velocity wall boundary condition is based on a relation between wall shear and velocity gradient in terms of either a skin friction coefficient; or the direct specification of the shear distribution.

The wall boundary condition on the total enthalpy may be used to account for the affect of cooling the duct by means such as regenerative cycling of the fuel. This is done by explicitly specifying the wall temperature and computing the local enthalpy from it. Alternatively, the wall may be considered to be isoenergetic.

Wall Drag

In the present formulation the value of C_f or τ_w must be specified. This can be done in several ways. For example a mixing chamber calculation can be performed assuming $C_f=0$. The wall

property distributions thereby generated constitute the edge conditions to be employed in an existing boundary layer calculation to determine the shear distribution τ_w. The mixing calculation is now repeated with the non-zero shear. If, in fact, the shear is small and the total friction drag is negligible compared to the influx of momentum, it would not be necessary to go beyond this first iterate. An alternative approach involves a more empirical approach, where C_f is an initially specified constant.

Now, C_f is a function of the local Reynolds number, Mach number, wall and boundary layer edge temperatures as well as the pressure gradient. However, for sufficiently high Reynolds numbers and mild adverse pressure gradients, C_f is rather a weak function of x. Thus, for a preliminary assessment of the boundary layer effect a constant value of C_f would be adequate. For example, based on a comparison with the experiments in Reference 10 , a value of $C_f/2 = 1.5 \times 10^{-3}$ was found to give good agreement for a range of conditions characteristic of ejector ramjet type flows. It should be noted that the current version of the computer program requires specification of a constant value of C_f only.

Chamber Geometry

To provide the versatility necessary for both analysis of existing hardware and design of new hardware, either the wall contour or the axial pressure distribution may be specified. Thus, one may specify:

$$y = y\ (x)$$

or

$$p = p\ (x)$$

The unspecified variable becomes a dependent quantity, and is given as part of the solution.

The solution technique is based upon an explicit finite difference method and is detailed in References 6 and 7. Some of the essential features are given in Appendix B.

Equilibrium Chemistry Models

In defining the chemical species to be considered as part of a hydrocarbon-air equilibrium chemistry package, attention was given to choosing species that would be representative of those formed as the result of a pyrolysis or cracking process which is of potential importance in a regenerative cycle for cooling purposes. Thus, in addition to the species H, O, H_2O, O_2, OH, CO, CO_2, and N_2, which are commonly considered as typical of high temperature hydrocarbon combustion products, CH_4, C_2H_2, C_2H_4, C_2H_6, $C_{(g)}$, and $C_{(s)}$ were included in the system. In addition the numerical analysis was set up so that the fuel specie could be chosen from among CH_4, C_2H_2, C_2H_4, C_2H_6, C_3H_8, C_3H_6, C_4H_8, C_4H_{10}, C_6H_6, and C_9H_{20}. It is felt that this relatively small chemical system (of never more than sixteen species at one time) is a representative equilibrium model of hydrocarbon combustion processes at both low and high temperatures, and for highly fuel rich as well as fuel lean mixtures.

The method of numerical solution is a standard technique involving the minimization of Gibbs Free Energy by means of "the method steepest descent." Care was taken in the writing of the computer program to construct a system which did not require any but the most arbitrary initial guesses for the chemical species.

Typical results from flame temperature calculations are shown in Figures 3 and 4.

In the course of developing the equilibrium chemistry model, and coupling it to the mixing analysis, the usefulness of simple complete combustion models become apparent.

The standard complete combustion model for a hydrocarbon-oxygen system is:

$$C_nH_m + pO_2 \rightarrow nCO_2 + m/2\ H_2O + q \begin{cases} O_2 \text{ - fuel lean} \\ C_nH_m \text{ - fuel rich} \end{cases}$$

Obviously, this model ignores the effects of dissociation. For fuel-lean mixtures with flame temperatures less than 2500°K this simple model is an acceptable approximation to the equilibrium composition. For fuel-rich mixtures the above model is not as satisfactory, since CO and $C_{(s)}$ are present in significant amounts at equilibrium. A study of hydrocarbon-air equilibrium compositions tabulated in Reference 11 indicated that it would be possible to formulate a simple, algebraic fuel-rich "quasi-complete combustion" model by using three distinct regions of fuel/air ratios.

This type of simple, approximate equilibrium model is of interest, since in performing a typical combustion system multi-dimensional turbulent flow field calculation using a digital computer, most of the computer running time is usually spent performing the chemistry calculation. This is true even when an equilibrium chemistry model rather than a finite-rate chemistry model is employed. For many applications the chemistry effects are of prime importance and must be modelled to as high a degree of accuracy as possible.

However in making preliminary design studies for a proposed propulsion system, it is always desirable to investigate the extremes of no burning ("frozen chemistry") and maximum burning ("complete combustion chemistry"). Thus it was decided to attempt to develop "quasi-complete combustion" models that would be appropriate for fuel-rich as well as fuel lean mixtures.

The first attempt to formulate the model is shown in Figure 5. This model yields flame temperatures that are only slightly above that at true equilibrium. However, the representation of the relative amounts of the major chemical species in zones A and B was not very realistic for most combinations of pressure and initial mixture temperature. This led to a revision of zones A and B, resulting in the model shown in Figure 6. In particular, the entire spectrum of equivalence ratios is modeled by four distinct regimes defined according to the fuel-to-oxygen atom ratio.

In this lean regime complete oxidation of the fuel forming CO_2 and H_2O is assumed. The upper limit for this regime is the stoichiometric point where the atom balance is given by:

$$\tfrac{1}{2}\,\tilde{Y}_H + 2\tilde{Y}_C = \tilde{Y}_O$$

where $\tilde{Y}$'s are the atom concentrations. In terms of element mass fractions this relationship is given by:

$$\tfrac{1}{2}\,\frac{\tilde{\alpha}H_2}{WH_2} + \frac{\tilde{\alpha}_C}{Wc} = \frac{\tilde{\alpha}O_2}{WO_2}$$

Accordingly, the lean regime is defined within the limits:

$$\frac{\tilde{\alpha}O_2}{WO_2} \geq \tfrac{1}{2}\,\frac{\tilde{\alpha}H_2}{WH_2} + \frac{\tilde{\alpha}_C}{Wc} \geq 0$$

and the specie mass fractions are given by:

$$\alpha_{H_2O} = \frac{\tilde{\alpha}H_2}{WH_2} \quad WH_2O$$

$$\alpha CO_2 = \frac{\tilde{\alpha}_c}{Wc} WCO_2$$

$$\alpha O_2 = \tilde{\alpha}O_2 - \tfrac{1}{2}\frac{\tilde{\alpha}H_2}{WH_2} - \frac{\tilde{\alpha}_c}{Wc} \quad WO_2$$

It is noted that the lean regime is represented by the standard complete combustion relationships.

In the fuel rich side it is observed that CO appears in substantial quantities and depending upon the degree of richness free hydrogen and finally solid carbon show up.

In zone A of Figure 6, it is found that the molar concentration of water is essentially constant and that carbon is oxidized to CO_2 and CO. This domain is bounded by the limits:

$$\tfrac{1}{2}\frac{\tilde{\alpha}H_2}{WH_2} + \frac{\tilde{\alpha}_c}{Wc} \geq \frac{\tilde{\alpha}O_2}{WO_2} \geq \tfrac{1}{2}\left(\frac{\tilde{\alpha}H_2}{WH_2} + \frac{\tilde{\alpha}_c}{Wc}\right)$$

wherein the species mass fractions are given by:

$$\alpha H_2O = \frac{\tilde{\alpha}H_2 WH_2O}{WH_2}$$

$$\alpha CO = WCO \left[2\left(\frac{\tilde{\alpha}_c}{Wc} - \frac{\tilde{\alpha}O_2}{WO_2}\right) + \frac{\tilde{\alpha}H_2}{WH_2}\right]$$

$$\alpha CO_2 = WCO_2 \left[2\frac{\tilde{\alpha}O_2}{WO_2} - \frac{\tilde{\alpha}_c}{Wc} - \frac{\tilde{\alpha}H_2}{WH_2}\right]$$

For a C_nH_m/O_2 system it is interesting to note that in zone A the mole fraction of water vapor, Y_{H_2O}, is 67% for olefins and something greater than this for the paraffins depending upon the size of the fuel molecule. Of course, the mass fraction, αH_2O, varies over this zone according to the local molecular weight of the products of combustion

In zone B free hydrogen begins to appear and the mole fraction of CO remains essentially constant. Hence, the bounds are:

$$\tfrac{1}{2}\left(\frac{\tilde{\alpha}H_2}{WH_2} + \frac{\tilde{\alpha}_c}{Wc} \right) \geq \frac{\tilde{\alpha}O_2}{WO_2} \geq \tfrac{1}{2}\,\frac{\tilde{\alpha}_c}{Wc}$$

and the species mass fractions are given by:

$$\alpha CO = \frac{\tilde{\alpha}_c WCO}{Wc}$$

$$\alpha H_2 = \alpha H_2 + WH_2 \left[\frac{\tilde{\alpha}_c}{Wc} - \frac{2\tilde{\alpha}O_2}{WO_2} \right]$$

$$\alpha H_2O = WH_2O \left[2\,\frac{\tilde{\alpha}O_2}{WO} - \frac{\tilde{\alpha}_c}{Wc} \right]$$

Here it is noted that the mole fraction of CO, Y_{CO}, is constant at 33% for olefins and something less for the paraffin series in a C_nH_m/O_2 system.

Finally in zone C the oxygen appears in CO only and free carbon forms. The mole fraction of hydrogen is essentially constant. This zone exists above the limit:

$$\frac{\tilde{\alpha}O_2}{WO_2} < \tfrac{1}{2}\,\frac{\tilde{\alpha}_c}{Wc}$$

and the species mass fractions are given by:

$$\alpha H_2 = \alpha H_2$$

$$\alpha CO = 2\alpha O_2 \frac{WCO}{WO_2}$$

$$\alpha C_{(s)} = \alpha_c - 2 \frac{\alpha O_2 Wc}{WO_2}$$

In this last regime, for a C_nH_m/O_2 system the mole fraction of hydrogen, Y_{H2}, is constant at 67% for olefins and something greater for paraffins again depending upon the molecular weight of the fuel This model, as shown in Figures 3 and 4, yields a flame temperature very near that of equilibrium except for mixtures very close to stoichiometric. In this region, the flame temperatures are high enough so that chemical dissociation is significant and hence the flame temperature of the complete combustion model is noticeably higher than the flame temperature at true equilibrium.

It should be noted that methane (CH_4) is a significant equilibrium specie in very fuel rich regions ($O/F < 1$ or $\phi > 3$) for fuels such as kerosene (C_9H_{20}), and that at low temperatures in highly fuel rich regions the original fuel specie is present at equilibrium in significant amounts rather than being completely broken down into $C_{(s)}$ and H_2. In summary, the quasi-complete combustion chemistry model is not a substitute for an equilibrium chemistry model. Instead, it is a useful approximate model when employed in making parameter studies, or in applications where the details of the combustion process are of secondary importance.

Turbulent Transport Viscosity Models

In general, the initial mixing region is a free shear layer and is bounded by the potential core on the inside and the secondary stream on the outside. Initially, this mixing region is essentially two-dimensional and the growth of the mixing layer varies linearly with the streamwise coordinate. In this region of the flow a Prandtl form for the eddy viscosity was employed:

$$0 \le x \le_{pc};\ \mu_{pc} = k_1 \rho_e x \left| u_{\mathfrak{C}} - u_e \right| + 1 \times 10^{-4} \left(\frac{\text{lbf-sec}}{\text{ft}^2} \right)$$

where k_I is a constant and was determined by analysis of the experiments in Reference 10. It was found that a value of $k = 4 \times 10^{-4}$ provides a good representation of the experiments which were analyzed.

At the end of the potential core region the flow becomes a fully developed turbulent flow and a different viscosity representation is required. In this region of the flow, the model employed in Reference 12 was found to be adequate:

$$x_{pc} < x;\quad \mu = 1 \times 10^{-4} + k_2 r_{\frac{1}{2}} (\rho u)_{\mathfrak{C}} \left(\frac{\text{lbf-sec}}{\text{ft}^2} \right)$$

where k_2 is a constant and $r_{\frac{1}{2}}$ is the "half radius" defined by the location of the mean mass flux (ρu) across the duct. The value of k_2 was found by working with experimental data to be $k = .018$.

Since the analysis may also be used for investigating free jet and plume problems, appropriate viscosity models (described in References 7 and 13) have also been included in the computer program. (Table II).

Since finite-rate condensation and solid carbon are included in the analysis, the question of to what degree the presence of

a particulate phase will affect the mixing process, and the eddy models used in describing it has been considered. In general, it can be expected that any particles present in the flow field, whether they result from the formation of soot in highly fuel-rich regions, or the condensation of water in locally low temperature areas, will have diameters of the order of 1 micron, or less. For particles this small, the assumptions of thermal and dynamic equilibrium may be made. Following References 14 and 15, the relation between the gaseous and the mixture turbulent viscosities is

$$\frac{\mu_t}{\mu_{tg}} = 1 + \frac{\sum_j^{\text{condensed}} \frac{\epsilon_p^j}{\epsilon_g} \alpha_p^j}{\alpha_g}$$

where ϵ_p and ϵ_g are the diffusivities of the particles and gas, respectively.

For micron sized particles

$$\epsilon_p/\epsilon_g \simeq 1$$

and hence,

$$\frac{\mu_t}{\mu_{tg}} \cong 1 + \frac{\alpha_p}{\alpha_g} = \frac{1}{\alpha_g}$$

Thus,

$$\mu_t \cong \frac{\mu_{tg}}{\alpha_g}$$

and the local eddy viscosity may be computed by using the existing gas phase models modified according to the above prescription. Input formats for the various versions of the parabolic programs are given in Appendix A.

B. Hyperbolic and Mixed Hyperbolic/Parabolic Flows in Augmentation Chambers, Scramburners and Nozzles

There are a number of practical propulsion systems whose internal flows cannot be adequately described by equations based upon purely boundary layer considerations. Examples of such systems include scramburners and composite engines where the flow is either supersonic throughout or mixed supersonic/subsonic, respectively. The work described in Section A was based upon the treatment of flows described by parabolic equations and is applicable to flows at Mach numbers in the range $0 < M < 0(2)$. At higher Mach numbers disturbances will propagate through the flow and the assumption that the pressure is constant normal to the local flow direction is no longer valid.

What is required for these flows is an analysis which includes lateral pressure variations in addition to mixing and combustion. In previous work a technique was developed for the solution of the viscid-inviscid equations for supersonic flows, with mixing and combustion, c.f., References 9 and 16 . Although that work considered only supersonic flows the solution technique used there may be extended in a relatively straight forward manner to mixed flows. The solution technique involves a composite of hyperbolic and parabolic concepts. A characteristics calculation is performed across a step for the local pressure and flow deflection. Then a diffusion/combustion calculation is carried out within the step for velocity, temperature and species concentrations. The characteristics calculation incorporates the effects of diffusion and combustion in the compatibility equations. This requires that the diffusion and combustion effects be treated as part of the forcing function in the compatibility equations. Therefore, there is a lag in the calculations over the step. This provides a mechanism for iterating, on say, the pressure by repeating the characteristics calculation

with an updated forcing function. This is done until the pressure no longer changes (to within a prescribed tolerance). This has shown to be a feasible solution technique for free and ducted flows with and without combustion in References 16 and 17.

Assuming, for the mixed flows of interest here, that diffusion is important only normal to the streamlines, or primary flow direction, then, one need only bypass the characteristic "leg", when performing the calculation within the low speed region of the flow. Thus, the flow field is considered to be made up of two regimes:

1. The high speed regime described by the generalized equations referred to as the Method of Characteristics with Viscosity (MOCV), and
2. The moderate to low speed regime described by purely parabolic equations.

This concept is shown in Figure 7.

The equations and solution procedure for the mixed flow problem is described below. It should be noted, however, that this formulation contains the pure supersonic flows as an inherent subsystem. Referring to Figure 8, the describing equations are:

<u>Global Continuity</u>

$$(\rho q)_s + \frac{j\rho q}{r} \sin\theta + \rho q \theta_n = 0 \qquad (1)$$

<u>s-Momentum</u>

$$\rho q\, q_s + P_s = \frac{1}{r^j} \left[r^j \mu \frac{\partial q}{\partial n} \right]_n \qquad (2)$$

<u>n-Momentum</u>

$$\rho q^2 \theta_s + P_n = 0 \qquad (3)$$

Species Continuity

$$\rho q(\alpha_i)_s = \rho \dot{W}_i + \frac{1}{r^j}\left[r^j \mu \frac{Le}{Pr} (\alpha_i)_n\right]_n \tag{4}$$

Energy

$$\rho q H = \frac{1}{r^j}\left[r^j \frac{\mu}{Pr} H_n\right]_n + \frac{1}{r^j}\left[\left(1-\frac{1}{Pr}\right)\mu (q^2/2)_n\right]_n + \frac{1}{r^j}\sum_i \left[(Le-1) r^j \frac{\mu}{Pr} h_i (\alpha_i)_n\right]_n \tag{5}$$

where

$$H = \sum_i \alpha_i h_i(T) + q^2/2 \tag{6}$$

$$\rho = \frac{P}{RT \sum_i \frac{\alpha_i}{W_i}} \tag{7}$$

$$h_i = h_i(\alpha_i, T) \tag{8}$$

These equations are combined to yield two compatibility equations, relating changes in p and θ,

$$\frac{d\tau}{d\ell} \pm b \frac{dp}{d\ell} = \pm g \tag{9}$$

$$b = \frac{1 + \tau^2}{\rho q^2 \operatorname{Tan}\epsilon} \qquad \tau = \operatorname{Tan}\theta \tag{10}$$

$$g = \frac{(1+\tau^2)\sin\epsilon}{F} \left[\frac{\mu}{\rho q} \left(H_{nn} + \frac{\cos\theta}{y} H_n\right) - \frac{\mu}{p}\left(1 + \frac{F}{q^2}\right) \right. \tag{11}$$

$$\left. \left\{ q_{nn} + \frac{q_n \cos\theta}{y} \right\} - \sum_i h_i D_i + \frac{\rho RTF}{p} \sum_i \frac{D_i}{W_i} - \frac{F \sin\theta}{y} \right]$$

$$D = \frac{\mu}{\rho q} \alpha_{inn} + \frac{\mu}{\rho q} \frac{\cos\theta}{y} \alpha_{in} + \frac{\dot{W}_i}{q} \tag{12}$$

Equations 9 are solved along the two characteristics respectively inclined at the angles $\pm \epsilon_k$ to the streamline direction. The ϵ_k are given by:

$$\text{Tan } \epsilon_{1,2} = \pm \sqrt{\frac{F}{\rho q^2 \left(\frac{F}{p} - \frac{1}{\rho} - \frac{F}{\rho q^2} \right)}} \tag{13}$$

where

$$F = T \sum_i \alpha_i \frac{dh_i(T)}{dT} \tag{14}$$

and $\dot{W}_i$ represents the rate of production of the ith species as a result of chemical reactions and is a known function of species concentrations, temperature, and density.

Equations (1)-(8) comprise eight equations* for the eight dependent variables, p, ρ, T, H, h, q, θ, α_i. Of the five partial differential equations, Equations (1) - (5), the two compatibility equations (Equation (9)) are used in place of the global continuity and the normal momentum equations, and comprise the "hyperbolic" part of the system. Then the streamwise momentum, energy, and species continuity equations (Equations (2),(5),(4)) integrated along streamlines, comprise the "parabolic" part of

*For convenience we will refer to all the species continuity equations as one equation.

the system. They are solved by an explicit finite difference procedure, as are the characteristic compatibility equations. Referring to Figure 9, the computational procedure is as follows:

Consider the solution to be known at some axial station x. Then a characteristic mesh can be drawn, as sketched. Associated with this mesh is a minimum range (Δx) of influence.

First the compatibility equations are solved on the characteristic mesh (with uneven axial spacing). Then, by interpolations on p and θ, the ordinate, inclination, and pressure at $x + \Delta x$ of the streamlines originating at x are determined. With the pressure gradient known, the parabolic part of the system is solved in the sequence: streamwise momentum, energy, and species continuity.

Since the parabolic equations are subject to a stability limited step size which may be smaller than Δx, several "parabolic" steps may be taken for each characteristic step. The solution of the subsonic (completely "parabolic") region is obtained by deleting the characteristics solution from the MOCV computation. The normal pressure gradient in the subsonic region is considered zero, i.e., $p_n=0$, and the streamwise pressure gradient in that region is determined by matching the flow along the streamline, $\overline{AB}$, separating the two regions. This is done by relating

(a) pressure - deflection from the supersonic side, and

(b) pressure - area change from the subsonic side.

The relationship between (a) and (b) is established by conservation of mass in the "parabolic" regime. Now, with reference to Figure 10, the entire solution is known at the axial station, $x = x_n$. All the region below the right running characteristic $\overline{AC}$ is computed, as usual, by the Method of Characteristics with Viscosity. The ordinate y_B of the separating streamline, DSL, at x_{n+1} is given by

$$y_B^{n+1} = y_A^n + \int_{x_n}^{x_{n+1}} \frac{dy_{DSL}}{dx}\, dx$$

where dy_{DSL}/dx is replaced by some average value over the interval so that we can numerically evaluate the integral. As a first guess, we put $(dy/dx)_{DSL} = dy/dx)_A$ along the SSL. Then, by interpolating, we find the point D at $x = x_n$ whose running characteristic hits the point (x_{n+1}, y_B). With the value (initially guessed to be τ_A) for τ_B^* we can solve the compatibility equation along $\overline{DB}$ to obtain p_B^o, the initial guess for the pressure at B. Since $p_n = 0$ above $\overline{AB}$, we have the pressure in the entire parabolic region at x_{n+1}. Now we solve the parabolic part of the system obtaining the solution for the entire subsonic region, including point B, at x_{n+1}. The mass flow above A at x_n must equal that above B at $x_{n+1} = x_n + \Delta x$. Thus, by inverting the usual mass flow integration, the ordinates of all the streamlines above B, including y_F (the ordinate of the edge streamline $\overline{EF}$) are determined. Finally from the specified wall geometry, $y = y_{fs}\ (x_{n+1})$, a check is performed. In general, upon comparing y_F and y_{FS}, we do not find agreement. At this point we iterate on τ_B, the separating streamline inclination at B (and, implicitly, on y_B and p_B) until $y_F = Y_{FS}$ within some tolerance.

As an example of the technique, a calculation was performed for an <u>inviscid</u>, non-reacting mixed flow. The initial data consists of a supersonic core and a subsonic secondary. The upper wall is straight and parallel to the axis. The initial lateral pressure, Mach number, and flow deflection distributions

---

*τ = dy/dx, is the streamline slope.

(Figure 11) are specified to simulate typical flow conditions somewhat downstream of the initial merging between an under-expanded supersonic primary and a subsonic secondary. Then the flow downstream is computed, including the self-induced pressure gradient along the upper wall, by the procedure discussed above.

Figure 12 shows the distributions of pressure, temperature, density, and velocity in the "parabolic" regime, which in this case is fully subsonic. The results are compared with "NASA TR 1135". This comparison is made by entering into TR 1135 with the computed area distribution. The approach to the throat is of interest in this type of flow, and Figure 13 shows that the calculation procedure is able to approach close to the sonic point before it fails. Since no special treatment of the transonic flow is included this failure is to be expected. However, one can switch to a pressure specified mode and extrapolate through the choke point. In this case, the resulting area variation will be consistent with the fixed initial conditions. In general, one can use this procedure in conjunction with an adjustment of initial conditions until the area required to pass through the choke point is "essentially" equal to a specified chamber area distribution.

Although the basic technique has been formulated and tested, additional work is required. Inclusion of the chemical and phase kinetics packages are needed and constitutes part of the current effort under the present NASA Contract NAS8-21387.

III. APPLICATIONS AND SUMMARY

A. Applications

To demonstrate the spectrum of problems which can be described by the pure parabolic and MOCV analyses several examples are given below.

Rocket Motor Combustion Chamber

As an example of the type of flow fields that the parabolic system is applicable to, a set of computations were made for the Cornell Laboratory ethylene/oxygen (C_2H_4/O_2) rocket motor. The motor and the operating conditions are shown in Figure 14 and three calculations were made for those given set of conditions. The first two calculations were performed using the "quasi-global" finite rate combustion model previously reported in References 6 and 8. These calculations were made assuming; (a) chemical equilibrium over the entire injector face, and (b) equilibrium for the mid-ring, and unburnt reactants for the central and outer rings; thus, the mid-ring served as an ignition source. In the third case, the calculation was repeated using the first quasi-complete combustion model discussed in Section IIA. The purpose of performing these three calculations is to demonstrate the effect of chemical and initial flow modelling on the predicted chamber flow field. A comparison of the calculated exit conditions for the three configurations is shown in Figures 15 through 18. It may be seen that there is good agreement between the complete combustion calculation and the finite rate chemistry calculation assuming equilibrium for the entire injector face. For this motor, this suggests that if equilibrium was appropriate over the entire injector face then equilibrium, or in particular, complete combustion is adequate for predicting the flow field throughout the combustion chamber. However, the pilot ignition model gives a different result. This is due to two effects which differentiate this case from the first two calculations.

In the first place, the velocity profile across the injector face is not the same because of the unreacted state assumed for the central and outer streams. This difference effects the mixing rate which is particularly evident in the equivalence ratio profile at the end of the chamber, Figure 18.

The second difference is due to the ignition process which involves the propagation of the flame through the unburned propellents as the flow field develops.

This result suggests the importance of proper modeling of the initial conditions both fluid mechanically and chemically and indicates the relevance of the ignition mechanism in terms of the downstream flow field structure.

Nozzle Recombination

The analysis described under Section IIB is applicable to mixed, as well as pure supersonic flows. As an example of the applicability of the MOCV program to ducted flows, a study was made on an Atlas-Vernier rocket motor nozzle assuming inviscid flow. The engine was burning ethyl alcohol/water/LOX and the initial conditions at the throat are given in Table I and the nozzle contour is given by:

$$r = \begin{cases} 4.817 - \sqrt{16-x^2} \; ; & 0 < x \leq 1.0352 \text{ inches} \\ 0.67688 + 0.2679\, x; & 1.0352 \leq x \leq 4.69 \text{ inches} \end{cases}$$

where r is the nozzle radius, and x is the axial distance measured from the throat.

Two calculations were performed starting from the same equilibrium throat conditions. In the first the composition was assumed chemically frozen at the throat values. The second calculation considered finite rate recombination throughout the expansion from the throat to the exit plane.

Figures 19a and 19b show the centerline and wall velocity, pressure, and temperature distributions down the nozzle. Figure 20b show the H_2O and OH mass fraction distributions down the nozzle. The chemical system includes, in addition, O, H, O_2, H_2, CO, CO_2, N_2, $C_{(s)}$, and fuel but only the above two were shown. The exit profiles of T, p, and q are shown in Figure 21.

Special note should be made of the initial readjustment the in concentrations and temperature due to the transition from the specified equilibrium initial conditions to the finite rate kinetics calculation included in the MOCV. This is due to a combination of the assumption of equilibrium at the throat, and a possible mismatch in the equilibrium constants and the ratio of forward to backward reaction rate constants.

Proceeding down the nozzle one notes in the wall distributions, the effect of a change in wall slope at x = 1.0352 inches. The downstream effect of this appears to be essentially smeared out as indicated in the centerline distributions.

B. Summary

Analyses for the description of various combustion chamber and nozzle flows have been developed.

A parabolic analysis for low speed combustor including rocket motors is presented which includes coupled mixing, combustion and phase transition kinetics.

For applications involving mixed subsonic/supersonic or pure supersonic flows an analysis is presented which couples mixing, combustion, and lateral, as well as axial pressure variations. This analysis can treat scramburners, augmentation chambers and nozzles.

Examples of calculations are presented for a rocket combustion chamber and a nozzle recombination process.

The rocket motor study shows the potential value of complete combustion models for making rapid preliminary calculations. In addition, the results for the particular pilot ignition model using a kinetics mechanism shows the importance of proper modelling for the ignition process.

The nozzle recombination calculations demonstrate the capability to compute the throat to exit plane flow field using a single program which includes kinetics (and mixing) throughout. "Freezing" points are not a required input but rather are predicted as a natural consequence of the kinetics mechanism which is employed.

REFERENCES

1. "Performance Evaluation Methods for Liquid Propellant Rocket Thrust Chambers," ICRPG, CPIA Publication 132, November 1966.

2. "Handbook of Recommended Practices for Measurement of Liquid Propellant Rocket Engine Parameters," ICRPG, CPIA Publication 179, January, 1969.

3. Powell, W. B., "ICRPG Liquid Propellant Thrust Chambers Performance Evaluation Methodology," Journal of Spacecraft and Rockets, pp.105-108, January 1970.

4. Edelman, R.B., and Fortune, O.F., "An Analysis of Mixing and Combustion in Ducted Flows," AIAA Preprint No. 68-114, January 1968. Presented at the 6th Aerospace Sciences Meeting, January 1968, N.Y.

5. Edelman, R.B., and Fortune, O.F., "A Preliminary Analysis of Mixing and Combustion in Ducted Flows with Application to Ejector Ramjet Technology," GASL TR 658, May 1967.

6. Edelman, R.B., and Fortune, O.F., "Mixing and Combustion in the Exhaust Plumes of Rocket Engines Burning RP1 and Liquid Oxygen," GASL TR 631, November 1966.

7. Fortune, O.F., and Edelman, R.B., "The Effect of Mixing, Radiation, and Finite Rate Combustion Upon the Flow Field and Surroundings of the Exhaust Plumes of Rocket Engines Burning RP1 (Kerosene) and Liquid Oxygen," GASL TR 681, December 1967.

8. Edelman, R.B., and Fortune, O.F., "A Quasi-Global Chemical Kinetic Model for the Finite Rate Combustion of Hydrocarbon Fuels With Application to Turbulent Burning and Mixing in Hypersonic Engines and Nozzles," AIAA Preprint No. 69-86, Presented at the 7th Aerospace Sciences Meeting, N. Y. January 1969.

9. "Study on Reacting Gas Flows with Applications to Exhaust Plumes," Final Report, GASL TR 737, April 1970.

10. "Final Summary Technical Report - 1963 Ramjet Technology Program (U)", Vol. 2, "Jet Compressor Research and Ejector Ramjet Investigation," The Marquardt Co. Report No. 25-116.

11. General Electric Company, "Properties of Combustion Gases/ System = C_nH_{2n}-Air", McGraw Hill Book Co., 1955.

12. Edelman, R.B., "Diffusion Controlled Combustion for Scramjet Application - Part I - Analyses and Results of Calculations," GASL TR 569, December 1965.

13. Siegelman, D., and Fortune, O.F., "Computer Programs for the Mixing and Combustion of Hydrogen in Air Streams," GASL TR 618, July 1966.

14. Edelman, R.B., Schmotolocha, S., Slutsky, S., "Combustion of Liquid Hydrocarbon in a High Speed Air Stream," AIAA Preprint 70-88, Presented at the 8th Aerospace Sciences Meeting, N.Y., January 1970.

15. Edelman, R.B., "Turbulent Transport in Polydisperse Systems," GASL TR 735, 1970.

16. "Mixing and Combustion in Supersonic Flow With Lateral Pressure Gradient Effects," Final Report, GASL TR 636 August 1968.

17. Edelman, R.B., and Weilerstein, G., "A Solution of the Inviscid-Viscid Equations with Application to Bounded-Unbounded Multicomponent Reacting Flows," AIAA Preprint No. 69-83, January 1969, Presented at the 7th Aerospace Sciences Meeting, N. Y. 1969

APPENDIX A

INPUT FORMATS FOR PARABOLIC PROGRAMS WITH EQUILIBRIUM AND QUASI-COMPLETE COMBUSTION MODELS

DECK 7C

INPUT FORMAT FOR A FREE OR DUCTED FINITE DIFFERENCE MIXING PROGRAM WITH HYDROCARBON-AIR TWO-PHASE EQUILIBRIUM CHEMISTRY

CARD	COLUMN	FORMAT	DESCRIPTION
1	2-80	20A4	Title card; will be printed on every page of output
2	1-5	I5	Number of ψ grid points (M) ($\leq$ 50) at initial x
	6-10	"	Number of ψ grid points at x = 0 after grid size is halved ($\leq$ 25)
	11-15	"	Number of first viscosity model (from 1 to 8)
	16-20	"	Number of second viscosity model, if any
	21-25	"	input { 0 - Axisymmetric coordinates used; 1 - Plane two-dimensional
	26-30	"	input { 0 - Isoenergetic wall boundary condition; 1 - Wall temperature (^{o}K) specified
	31-35	"	input { 0 - Free jet problem with static pressure prescribed; 1 - Ducted problem with static pressure prescribed; 2 - Ducted problem with wall radius prescribed
	36-40	"	$\neq$ 0 is a printout dump for mixing process
	41-45	"	Used only with ducted, wall radius prescribed case. Input $\neq$ 0 adds refinement to pressure interation process.
	46-50	"	0 - no printout dump from equilibrium chemistry 1 - some printout dump from equilibrium chemistry 2 - ample printout dump from equilibrium chemistry 3 - overwhelming printout dump from equilibrium chemistry.
	51-55	"	This input specifies the hydrocarbon that will be considered to be the fuel.

Input	Fuel	Input	Fuel
11	CH_4	16	C_3H_6
12	C_2H_2	17	C_4H_8
13	C_2H_4	18	C_4H_{10}
14	C_2H_6	19	C_6H_6
15	C_3H_8	20	C_9H_{20}

DECK 7C (Contd)

	56-60	"	Input { 0 - Constant pressure/temperature equilibrium calculation is performed for input profile data. 1 - Constant pressure/ enthalpy equilibrium calculation is performed for input profile data.
3	1-10	E10.8	Printout interval (feet)
	11-20	"	Maximum axial distance (feet)
	21-30	"	Initial axial location (feet)
	31-40	"	Wall temperature (^{o}K) - only if specified above
4	1-10	E10.8	Lewis Number
	11-20	"	Prandtl Number
	21-30	"	$\Delta\psi$
	31-40	"	XMPS; $\Delta x = \Delta x$ /XMPS
	41-50	"	δ^* initial in viscosity models 7 and 8 (appropriate to plume problems) (feet)
	51-60	"	ψ_1; magnitude of lowest grid point
5	11-20	"	(a) $\frac{d\mu}{dx}$ in model 1 (linear buildup of viscosity) (lbf-sec/ft^3)
			(b) Value of μ in model 6 (constant viscosity) (lbf-sec/ft^2)
			(c) $\delta^*_{initial}$ if model 7 or 8 is used as second viscosity model (feet)
	21-30	"	(a) Endpoint (x) of model 1(feet)
			(b) Initial jet width in model 5(potential core model) (feet)
	61-70		Standard width (feet) for printout purposes
6	1-10	"	Initial wall radius (feet) for pressure prescribed case, or initial pressure (lbf/ft^2) for wall radius prescribed case.
	11-20	"	x_1, x_2, x_3 } End points (feet) of pressure or wall radius polynomials
7	1-10	"	a_1, a_2, a_3, a_4, a_5, a_6, x^* } First pressure (lbf/ft^2) or wall radius (ft) polynomial $F_1(x)=a_1+a_2(x-x^*) + \ldots+a_6(x-x^*)^5$

DECK 7C (Contd)

8	1-70	E10.8	Second P or y_w polynomial	
9	1-70	"	Third P or y_w polynomial	
10	1-70	"	Fourth P or y_w polynomial	
11a	1-10	E10.8	$T(\psi_1)$	Initial static temperature profile (^oK)
	11-20	"	$T(\psi_2)$	
	--			
	61-70	"	$T(\psi_7)$	
11b	1-10	"	$T(\psi_8)$	
	11-20	"	$T(\psi_9)$	
	--		--	
			$T(\psi_M)$	
12a	1-10	E10.8	$U(\psi_1)$	Initial velocity profile (feet/second)
	--			
	61-70	"	$U(\psi_7)$	
12b	1-10	"	$U(\psi_8)$	
	--		--	
			$U(\psi_M)$	
13Aa	1-10	E10.8	α_H	Species mass fractions at ψ_1. Three cards are inputted for each grid point.
	11-20	"	α_O	
	21-30	"	α_{H_2O}	
	31-40	"	α_{H_2}	
	41-50	"	α_{O_2}	
	51-60	"	α_{OH}	
	61-70	"	α_{CO}	
13Ab	1-10	"	α_{CO_2}	
	11-20	"	α_{N_2}	
	21-30	"	$\alpha_{C(gas)}$	
	31-40	"	α_{CH_4}	
	41-50	"	$\alpha_{C_2H_2}$	
	51-60	"	$\alpha_{C_2H_4}$	

DECK 7C (Contd)

13Ab	61-70	E10.8	$\alpha_{C_2H_6}$	Species mass fractions at ψ_1. Three cards are inputted for each grid point.
13Ac	1-10	"	$\alpha_{C_NH_M}$ (Fuel)	
	11-20	"	$\alpha_{C(solid)}$	
13Ba 13Bc			Mass fractions at ψ_2	
... 13Ma			Mass fractions at ψ_M	

Deck 9

Input Format for a Free or Ducted Finite Difference Mixing Program with Hydrocarbon-Air Two-Phase Quasi-Complete Combustion Chemistry with Finite Rate Condensation of Water or Carbon Dioxide.

Card	Card Column	Format	Description
1	2-72	12A6	Title card; will be printed on every page of output
2	1-5	I5	Number of ψ grid points (M) ($\leq$ 50) at initial x
	6-10	"	Number of ψ grid points to be retained after grid size is halved ($\leq$ 25)
	11-15	"	Number of first viscosity model used (from 1 to 8)
	16-20	"	Number of second viscosity model used if any.
	21-25	"	Input { 0 - Axisymmetric coordinates used; 1 - Plane 2-Dimensional coordinates }
	26-30	"	Input { 0 - Isoenergetic wall boundary cond.; 1 - Wall temperature is an input }
	31-35	"	Input { 0 - free jet problem with static pressure prescribed.; 1 - Ducted problem with static pressure prescribed; 2 - Ducted problem with wall radius prescribed. }
	36-40	"	$\neq$ 0 is a printout dump for mixing process.
	41-45	"	$\neq$ 0 is a printout dump for condensation process.
	46-50	"	Number of condensation model used (from 1 to 6)
	51-55	"	Input { 0 - Condensed particles not initially present; 1 - Condensed particles initially present; Must input mass fractions and radii }
	56-60	"	Input { 0 - Condensate considered to be CO_2; 1 - Condensate considered to be H_2O }
3	1-10	E10.8	Printout interval (feet)
	11-20	"	Maximum axial distance (feet)
	21-30	"	Initial axial location (feet)
	31-40	"	n { atom numbers in chemical species that
	41-50		m { is considered as the fuel: C_nH_m
	51-60	"	Wall temperature (^oK), if specified.

Deck 9 (Contd)

Card	Card Column	Format	Description
4	1-10	E10.8	Lewis Number
	11-20	"	Prandtl Number
	21-30	"	$\Delta\psi$
	31-40	"	XMPS; Δx /XMPS
	41-50	"	δ^* initial in viscosity models 7 & 8 (appropriate to plume problems) (feet)
	51-60	"	ψ_1; magnitude of lowest grid point
5,6,7	Three cards with thermodynamic data for the specific fuel, C_nH_m, being used.		
8	1-10	E10.8	R_1
	11-20	"	R_2
	21-30	"	R_3
	31-40	"	R_4
	41-50	"	R_5
	51-60	"	R_6 } Upper limits (feet) of condensate droplet radius permitted in each of the ten classes of droplets.
	61-70	"	R_7
9	1-10	"	R_8
	11-20	"	R_9
	21-30	"	R_{10}
10	11-20	"	(a) $\frac{d\mu}{dx}$ in model 1 (linear buildup of viscosity) (lbf-sec/ft^3)
			(b) Value of μ in model 6 (constant viscosity) (lbf-sec/ft^2)
			(d) $\delta^*_{initial}$ if model 7 or 8 is used as second viscosity model (feet)
	21-30	"	(a) Endpoint (x) of model 1 (feet)
			(b) Initial jet width in model 5 (potential core model) (feet)
	61-70	"	Standard configuration width (feet)
11	1-10	"	Initial wall radius (feet) for pressure prescribed case, or initial pressure (lbf/ft^2)
	11-20	"	X_1
	21-30		X_2 } End points (feet) of pressure or wall radius polynomials
	31-40	"	X_3

Deck 9 (contd)

Card	Card Column	Format		Description
12	1-10	E10.8	a_1	First pressure (lbf/ft^2) or wall radius (ft) polynomial $F_1(x)=a_1+a_2(x-x^*)+\ldots+a_6(x-x^*)^5$
	11-20	"	a_2	
	21-30	"	a_3	
	31-40	"	a_4	
	41-50	"	a_5	
	51-60	"	a_6	
	61-70	"	x^*	
13	1-70	"		Second P or y_w polynomial
14	1-70	"		Third P or y_w polynomial
15	1-70	"		Fourth P or y_w polynomial
16a	1-10	"	$T(\psi_1)$	Initial static temperature profile (^oK)
	11-20	"	$T(\psi_2)$	
	--			
	61-70	"	$T(\psi_7)$	
16b	1-10	"	$T(\psi_8)$	
	11-20	"	$T(\psi_9)$	
	--	"	$T(\psi_M)$	
17a	1-10	"	$U(\psi_1)$	Initial velocity profile (feet/second)
	--		$U(\psi_7)$	
17b	1-10	"	$U(\psi_8)$	
	--		--	
			$U(\psi_M)$	
18Aa	1-10	"	α_H	Mixture species mass fraction at ψ_1 Two cards are input for each grid point.
	11-20	"	α_O	
	21-30	"	α_{H_2O}	
	31-40	"	α_{H_2}	
	41-50	"	α_{O_2}	
	51-60	"	α_{OH}	
	61-70	"	α_{CO}	

Deck 9 (contd)

Card	Card Column	Format		Description
18Ab	1-10	E10.8	α_{CO_2}	Mixture species mass fractions at ψ_1. Two cards are input for each grid point
	11-20	"	$\alpha_{C_nH_m}$	
	21-30	"	α_{N_2}	
	31-40	"	$\alpha_{Solid\ C}$,	
	41-50	"	$\alpha_{Condensate\ (CO_2\ or\ H_2O)}$	
18Ba			Mass fractions at ψ_2	
18Bb				
...			...	
18Ma			Mass fractions at ψ_M	
18Mb				

If, condensate droplets exist at the initial starting point of the computation, the initial mass fraction and particle radius must be given below for each of the ten classes of particles.

19Aa	1-10	E10.8	α_1	Mixture mass fraction of condensate (CO_2 or H_2O) in each category at ψ_1.
	11-20	"	α_2	
	21-30	"	α_3	
	31-40	"	α_4	
	41-50	"	α_5	
	51-60	"	α_6	
	61-70	"	α_7	
19Ab	1-10	"	α_8	
	11-20	"	α_9	
	21-30	"	α_{10}	
	31-40	"	r_1	Radius (ft) of condensate droplets in each category at ψ_1
	41-50	"	r_2	
	51-60	"	r_3	
	61-70	"	r_4	
19Ac	1-10	"	r_5	
	11-20	"	r_6	
	21-30	"	r_7	
	31-40	"	r_8	

Deck 9 (concld)

Card	Card Column	Format	Description
19Ac	41-50	E10.8	r_9 } Radius (ft) of condensate droplets
	51-60		r_{10} } in each category at ψ_1
19Ba			Category mass fractions and radii at ψ_2
19Bb			
19Bc			
...			
19Ma			Category mass fractions and radii at ψ_M
19Mb			
19Mc			

APPENDIX B

SOME FEATURES OF THE FINITE DIFFERENCE SOLUTION OF THE PARABOLIC EQUATIONS

The solution of the parabolic system has been obtained employing an explicit finite difference technique (Refs. 6 & 7). The finite difference formulation for the calculation of the flow at the point (n+1, M) is obtained by using the following explicit difference relations where P is anyone of the three pertinent variables u, $\tilde{\alpha}$; or H:

$$\frac{\partial P}{\partial x} = \frac{P_{n+1,M} - P_{n,M}}{\Delta x} \tag{15}$$

$$\frac{\partial P}{\partial \Psi} = \tfrac{1}{2}\,\frac{P_{n,M+1} - P_{n,M-1}}{\Delta \Psi} \tag{16}$$

$$\frac{\partial}{\partial \Psi}\left[b\,\frac{\partial P}{\partial \Psi}\right] = \frac{b_{n,M+\frac{1}{2}}\left[P_{n,M+1} - P_{n,M}\right] - b_{n,M-\frac{1}{2}}\left[P_{n,M-1}\right]}{\Delta \Psi^2} \tag{17}$$

where

$$b = \frac{\rho u y^{2N} \mu_t}{\Psi^N} \tag{18}$$

$$b_{n,M\pm\frac{1}{2}} = \tfrac{1}{2}\left[b_{n,M} + b_{n,M\pm 1}\right] \tag{19}$$

and

$$\Psi = M \cdot (\Delta \Psi) \tag{20}$$

The conservation equations in difference form are:

Elements:

M=0:

$$(\tilde{\alpha}_j)_{n+1,o} = (\tilde{\alpha}_j)_{n,o} + \frac{(1+N)\,2\,\Delta x}{(\Delta \Psi)^2}\left[\frac{(\rho u)^{1-N} Le_t \mu_t}{Pr_t}\right]_{n,o}\left[(\tilde{\alpha}_j)_{n,1} - (\tilde{\alpha}_j)_{n,o}\right] \tag{21a}$$

$M \neq 0$:

$$(\tilde{\alpha}_j)_{n+1,M} = (\tilde{\alpha}_j)_{n,M} + \frac{\Delta X}{M^N (\Delta\Psi)^{2+N}} \left\{ \left(\frac{Le_t b}{Pr}\right)_{n,M+\frac{1}{2}} (\tilde{\alpha}_j)_{n,M+1} - \right.$$

$$- \left[\left(\frac{Le_t b}{Pr_t}\right)_{n,M+\frac{1}{2}} + \left(\frac{Le_t b}{Pr_t}\right)_{n,M-\frac{1}{2}} \right] (\tilde{\alpha}_j)_{n,M} + \tag{21b}$$

$$\left. + \left(\frac{Le_t b}{Pr_t}\right)_{n,M-\frac{1}{2}} (\tilde{\alpha}_j)_{n,M-1} \right\}$$

j j^{th} element mass fraction

$$U_{n+1,o} = U_{n,o} + \frac{(1+N)2\ \Delta X}{(\Delta\Psi)^2} \left[(\rho u)^{1-N} \mu_t\right]_{n,o} [U_{n,1} - U_{n,o}] - \tag{22a}$$

$$- \frac{\Delta X}{(\rho u)_{n,o}} \left(\frac{dP}{dx}\right)_{n+1}$$

$M \neq 0$:

$$U_{n+1,M} = U_{n,M} + \frac{\Delta X}{M^N (\Delta\Psi)^{2+N}} \left\{ (b)_{n,M+\frac{1}{2}} U_{n,M+1} - \right.$$

$$\left. - [b_{n,M+\frac{1}{2}} + b_{n,M-\frac{1}{2}}] U_{n,M} + b_{n,M-\frac{1}{2}} U_{n,M-1} \right\} - \tag{22b}$$

$$- \frac{\Delta X}{(\rho u)_{n,M}} \left(\frac{dP}{dx}\right)_{n+1}$$

<u>Energy</u>:

$M=0$:

$$H_{n+1,o} = H_{n,o} + \frac{(1+N)2\Delta X}{(\Delta\Psi)^2} \left[(\rho u)^{1-N} U\right]_{n,o} \left\{ \left(\frac{1}{Pr_t}\right)_{n,o} [H_{n,1} - H_{n,o}] + \right.$$

$$+ \left(1 - \frac{1}{Pr_t}\right)_{n,o} \frac{1}{2} [U^2_{n,1} - U^2_{n,o}] + \tag{23a}$$

$$\left. + \sum_i \left(h_i \frac{Le_t - 1}{Pr_t}\right)_{n,o} [(\alpha_i)_{n,1} - (\alpha_i)_{n,o}] \right\}$$

$M \neq 0$

$$H_{n+1,M} = H_{n,M} + \frac{\Delta X}{M^N (\Delta\Psi)^{2+N}} \Bigg\{ \left(\frac{b}{Pr_t}\right)_{n,M+\frac{1}{2}} H_{n,M+1} - \left[\left(\frac{b}{Pr_t}\right)_{n,M+\frac{1}{2}} + \right.$$

$$\left. + \left(\frac{b}{Pr_t}\right)_{n,M-\frac{1}{2}}\right] H_{n,M} + \left(\frac{b}{Pr_t}\right)_{n,M-\frac{1}{2}} H_{n,M-1} + \left(b\left[1-\frac{1}{Pr_t}\right]\right)_{n,M+\frac{1}{2}} \frac{U^2_{n,m+1}}{2} -$$

$$- \left[\left(b\left[1-\frac{1}{Pr_t}\right]\right)_{n,M+\frac{1}{2}} + \left(b\left[1-\frac{1}{Pr_t}\right]\right)_{n,M-\frac{1}{2}}\right] \frac{U^2_{n,M}}{2} + \left(b\left[1-\frac{1}{Pr_t}\right]\right)_{n,M-\frac{1}{2}}$$

$$\frac{U^2_{n,M-1}}{2} + \sum_i \left[bh_i \left(\frac{Le_t-1}{Pr_t}\right)\right]_{n,M+\frac{1}{2}} (\alpha_i)_{n,M+1} -$$

$$- \sum_i \left[\left(bh_i \frac{Le_t-1}{Pr_t}\right)_{n,M+\frac{1}{2}} + \left(bh_i \frac{Le_t-1}{Pr_t}\right)_{n,M-\frac{1}{2}}\right] (\alpha_i)_{n,M} +$$

$$+ \sum_i \left[bh_i \frac{Le_t-1}{Pr_t}\right]_{n,M-\frac{1}{2}} (\alpha_i)_{n,M-1} \Bigg\} \tag{23b}$$

Step Size Control

The step size in the explicit finite difference scheme is controlled by a stability criterion and from studies of linear parabolic partial differential equations there results the following condition, Ref. 15:

$$\frac{\Delta\Psi^2}{(1+N)6} \left[\frac{Pr_t}{Le_t \mu_t (\rho u)^{1-N}}\right]_{n,o} \geq \Delta X \leq \frac{1}{3} \frac{M^N (\Delta\Psi)^{2+N}}{\left(\frac{Le_t}{Pr_t} b\right)_{n,M+\frac{1}{2}} + \left(\frac{Le_t}{Pr_t} b\right)_{n,M-\frac{1}{2}}} \tag{24}$$

Although the partial differential equations are non-linear, the present explicit difference formulation results in a locally linear system and Equation 24 provides an estimate of the stable step size. The computer program has as an input an arbitrary fraction which can be chosen to cut the above step size in the event a stability problem arises.

TABLE I

ATLAS VERNIER NOZZLE

R(ft)	.068
x(ft)	0
m	1.008
P(#/ft^2)	26.744
(fps)	2792.7
Mass Fractions	
CO	.24
CO_2	.33
H	5.89^{-4}
H_2	6.78^{-3}
H_2O	.3854
O	2.23^{-3}
O_2	1.155^{-2}
OH	2.3^{-2}
T(^{o}K)	3040.8
T(^{o}R)	5465
Molecular Weight	23.075
Note	Initial condition (throat)

TABLE II

TURBULENT VISCOSITY MODELS CONTAINED IN PARABOLIC MIXING PROGRAM

MODEL	FORM	COMMENTS
1	$\frac{x}{k_3}(k_2-10^{-4}) + 10^{-4}$	Domain: $0 < x < k_3$. This model is crude and has been used to assess mixing rates in the potential core region of concentric jets. Model 5 is recommended.
2	6.211×10^{-4}	Based on early work of Zakkay and has been used successfully for flame propagation studies in high speed premixed fuel/oxidizer systems.
3	$0.018 r_{\frac{1}{2}} (\rho u)_{\mathbb{C}} - (\rho u)_e + 10^{-4}$	Ferri model for fully developed unbounded two stream mixing.
4	$.0184_{\frac{1}{2}} (\rho u)_{\mathbb{C}}$	Zakkay model for fully developed mixing. Has been used successfully for bounded and unbounded flows.
5	$4 \times 10^{-4} \cdot \rho_e x \quad u_j - u_e + 10^{-4}$	Domain: $0 < x < 12 r_j \left[\frac{(\rho u)_j}{(\rho u)_e}\right]^{\frac{1}{2}}$ - Potential core model. Has been used successfully and it is recommended that it be coupled to Model 4.
6	k_2	Pure arbitrary constant - useful in developing computer programs.
7	$\left(\frac{x+\delta_i^*}{900}\right)[(\rho u)_j + (\rho u)_e] + 10^{-4}$	Shear layer model accounting for initial boundary effects.
8	$.01(L(x)+\delta_i^*)(\rho u)_j - (\rho u)_e + 10^{-4}$	Same as model 7 but does not assume a linear growth law for the mixing width. Here L(x) is computed as the flow field is generated.

Units $\equiv$ lb-sec/ft^2

$L(x) \equiv$ local width of mixing region

$r_{\frac{1}{2}} \equiv$ half radius determined at $(\rho u)_{r_{\frac{1}{2}}} = \frac{(\rho u)_{\mathbb{C}} + (\rho u)_e}{2}$

$\delta_i^* \equiv$ initial nozzle boundary layer displacement thickness

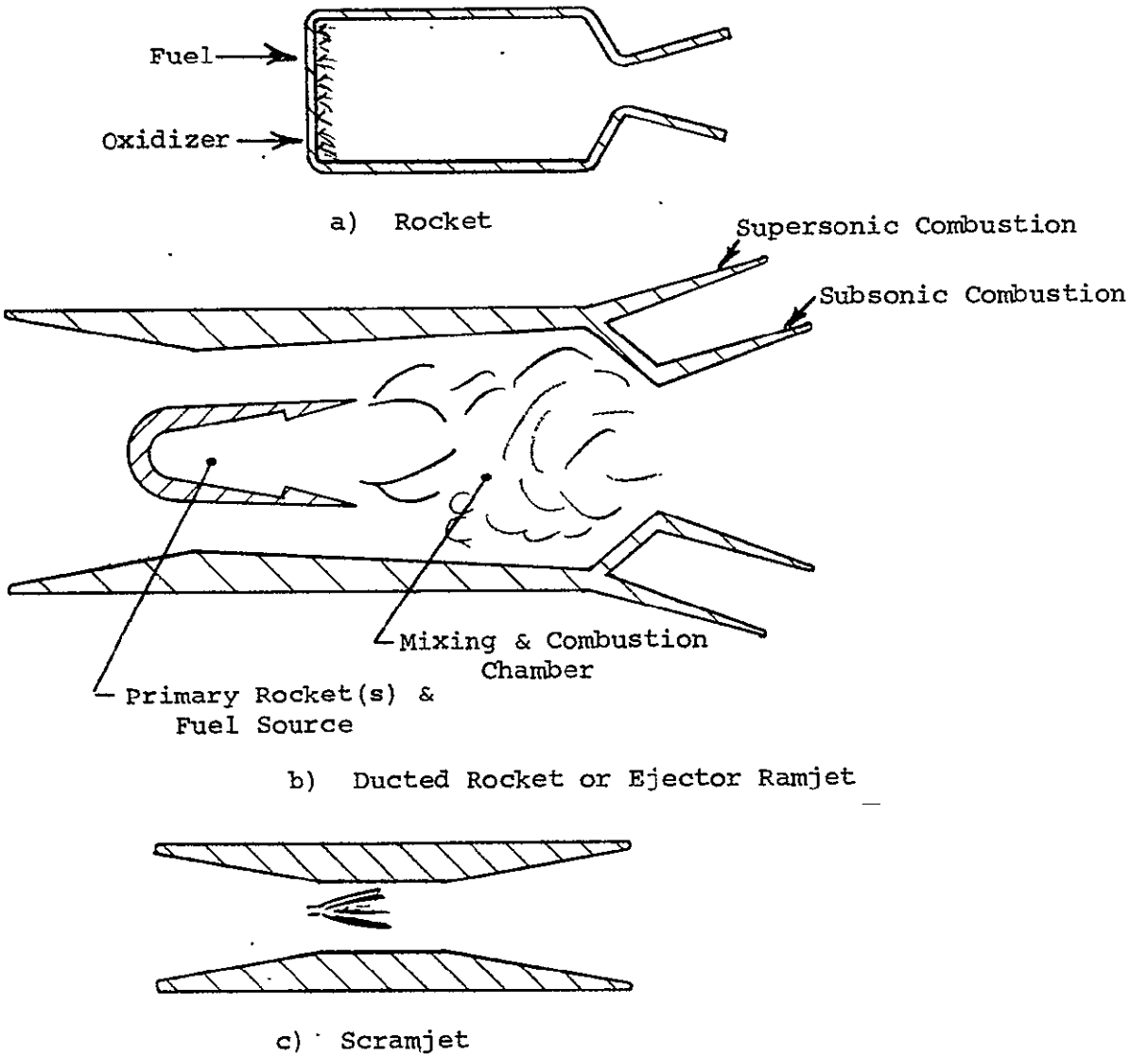

FIGURE 1 - SCHEMATIC OF PROPULSION SYSTEMS

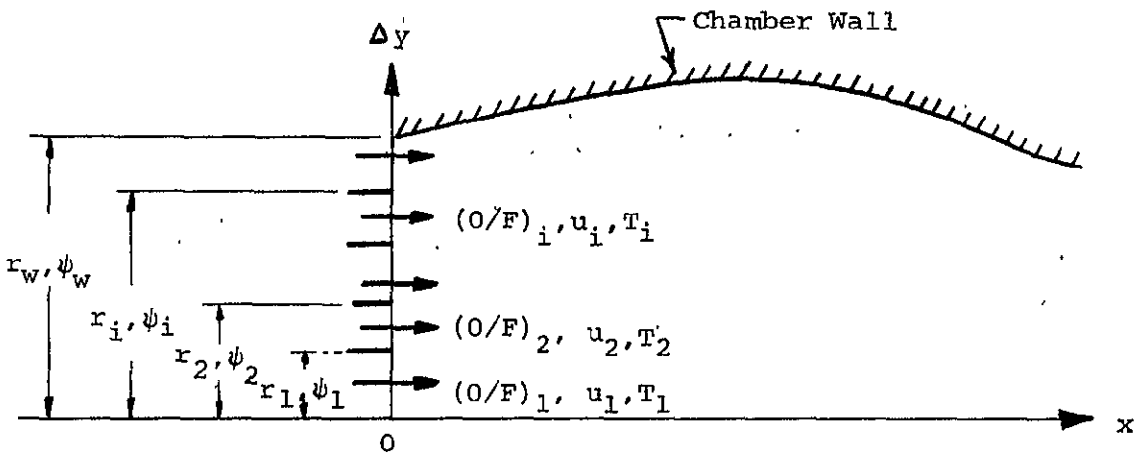

FIGURE 2 - SCHEMATIC OF ROCKET MOTOR COMBUSTION CHAMBER USING MULTIPLE RING INJECTION MODEL

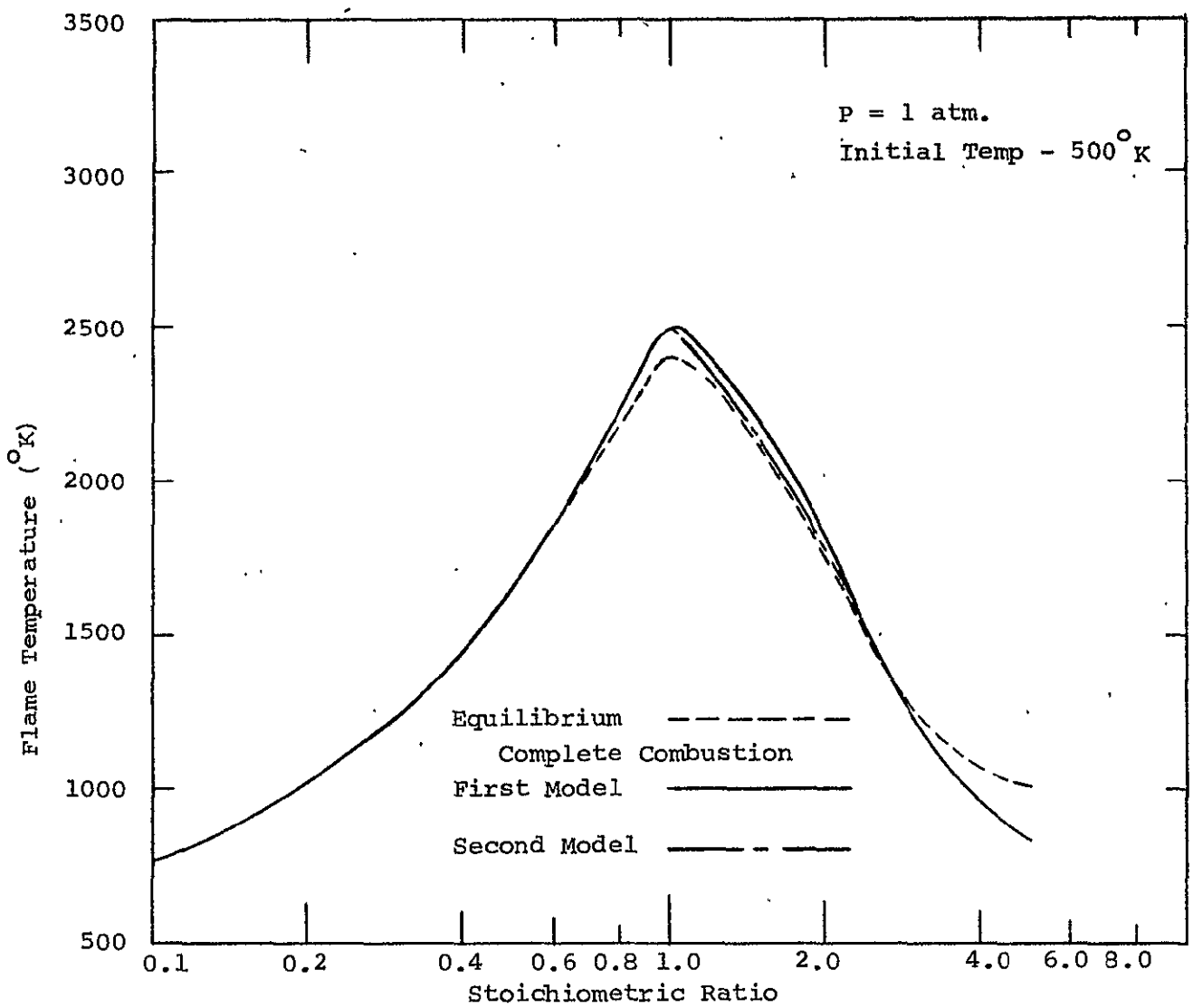

FIGURE 3 - COMPARISON OF QUASI-COMPLETE COMBUSTION MODELS WITH EQUILIBRIUM CHEMISTRY FOR A PROPANE-AIR SYSTEM

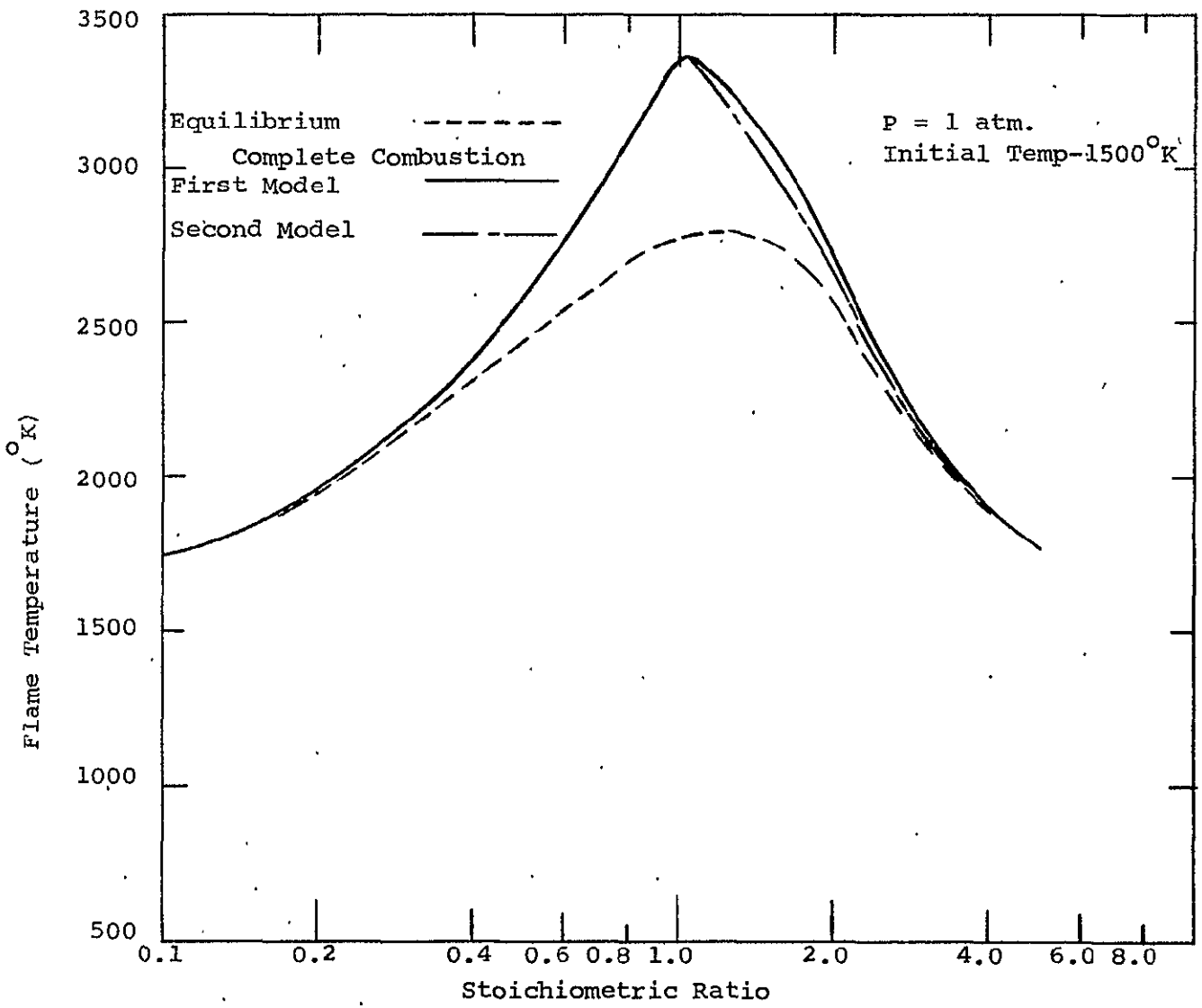

FIGURE 4 - COMPARISON OF QUASI-COMPLETE COMBUSTION MODELS WITH EQUILIBRIUM CHEMISTRY FOR A PROPANE-AIR SYSTEM

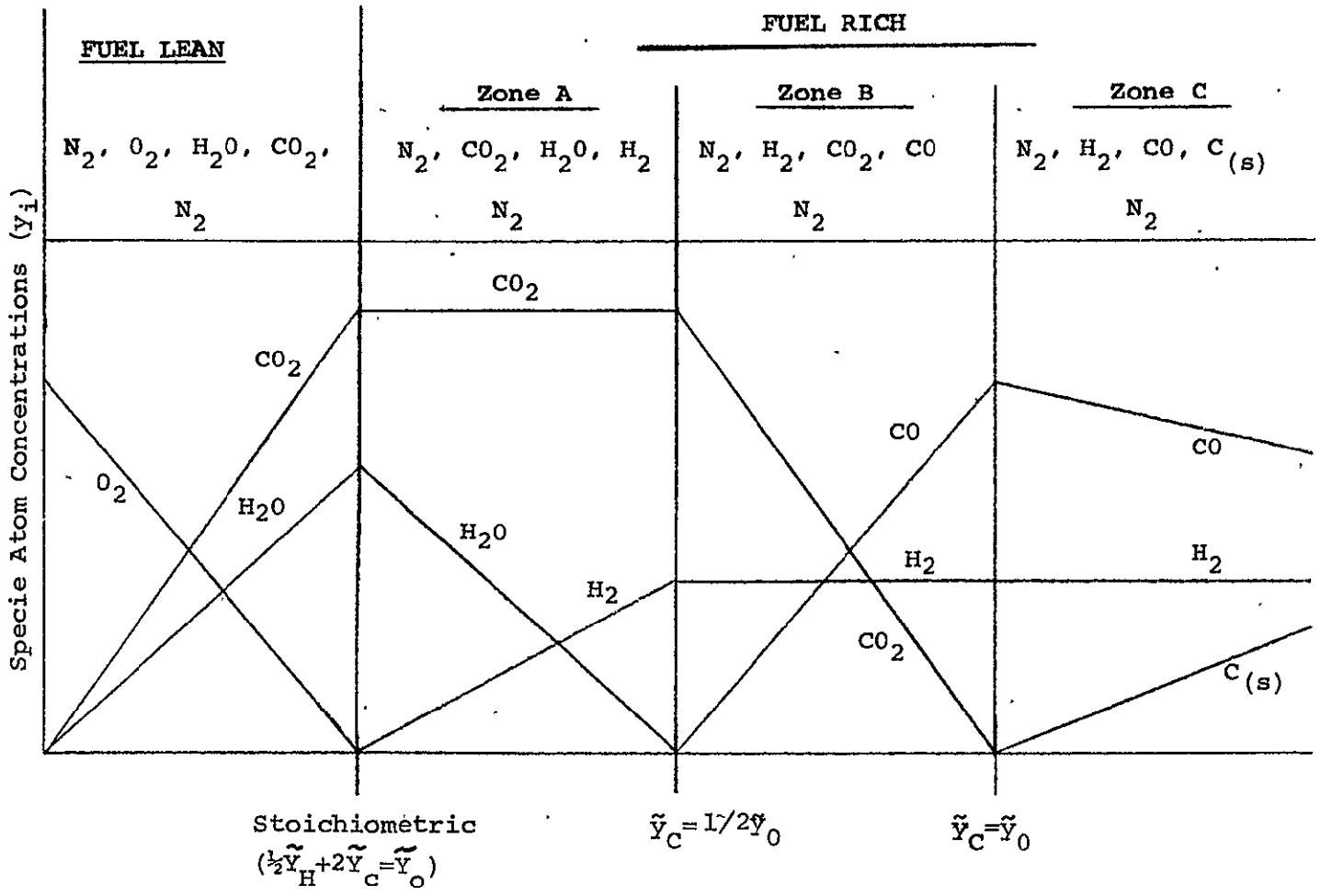

FIGURE 5. - EARLY QUASI-COMPLETE COMBUSTION OF HYDROCARBON-AIR CHEMISTRY MODEL (MODEL A)

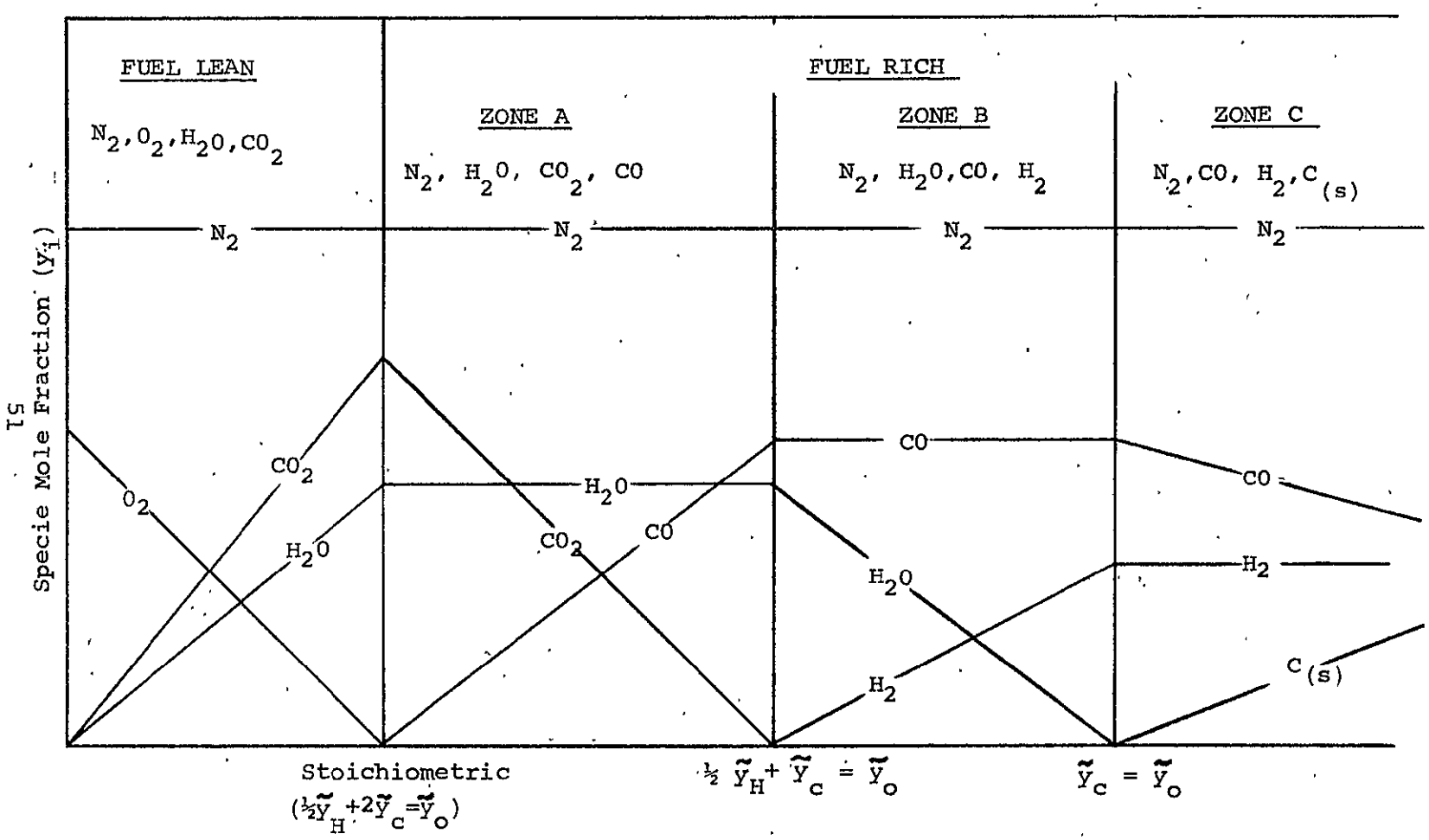

FIGURE 6 - FINAL QUASI-COMPLETE COMBUSTION HYDROCARBON-AIR CHEMISTRY MODEL (MODEL B)

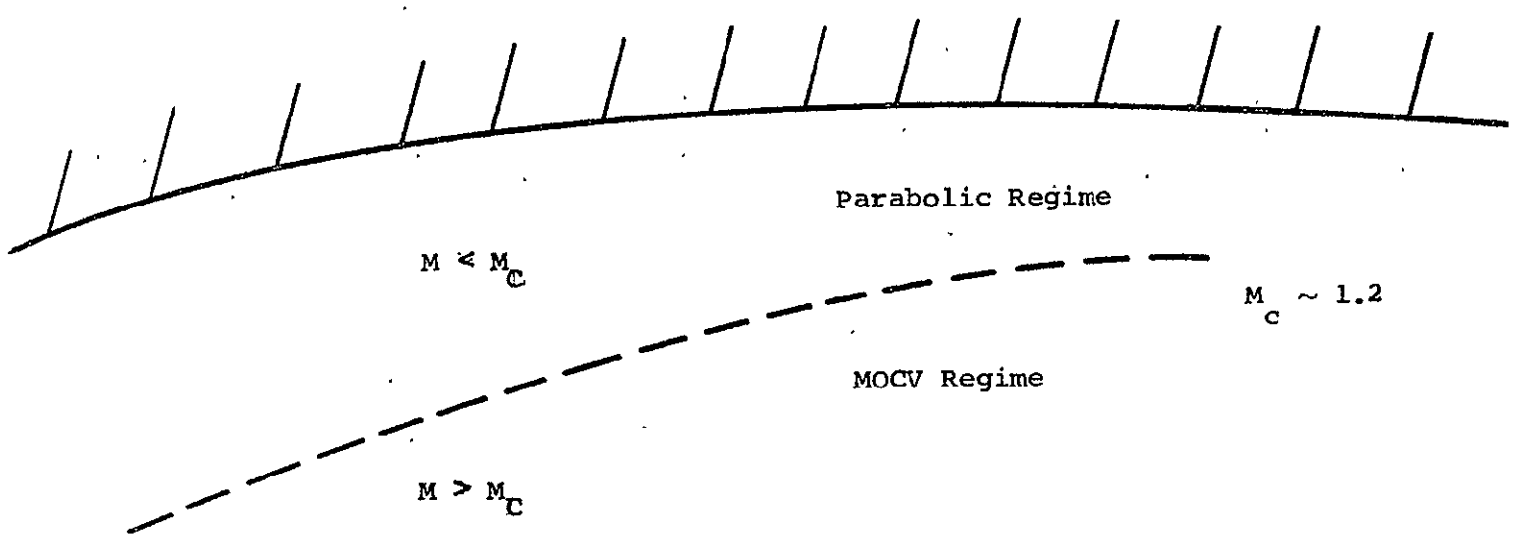

FIGURE 7 - SCHEMATIC OF MIXED FLOW CONCEPT

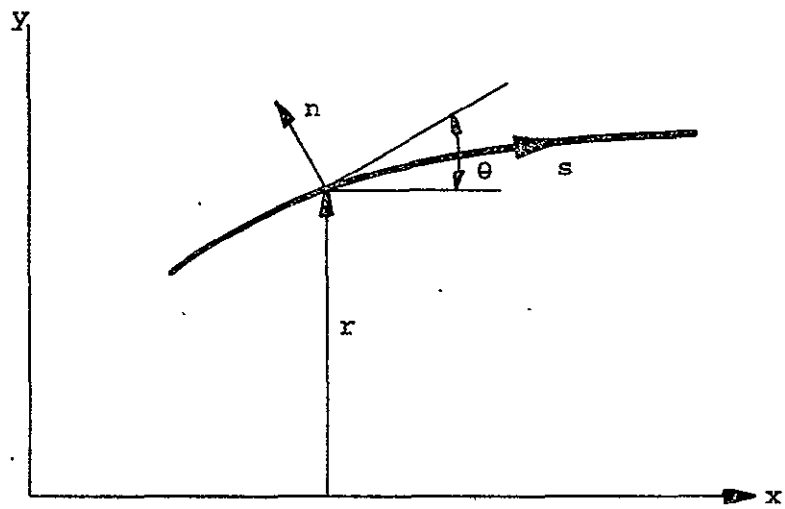

FIGURE 8 - INTRINSIC COORDINATE SYSTEM

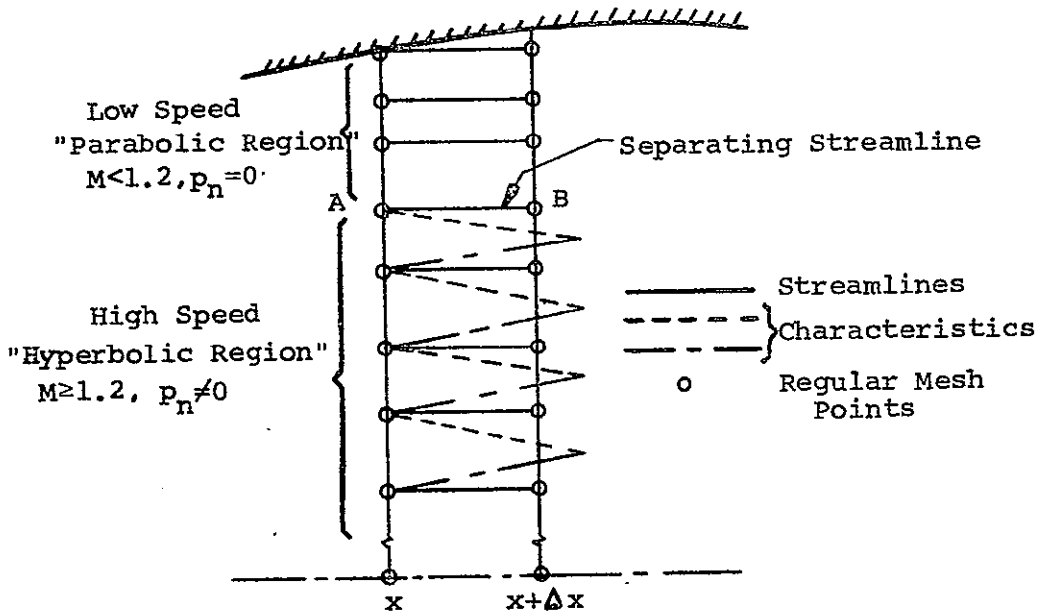

FIGURE 9 - COMPUTATION PROCEDURE

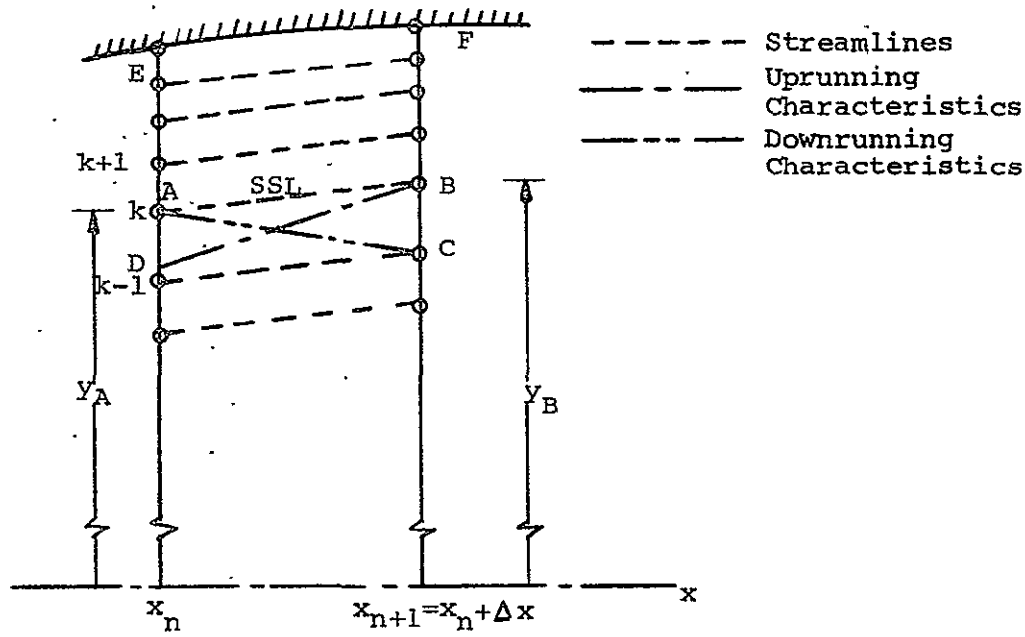

FIGURE 10 - PROCEDURE FOR MATCHING ALONG SEPARATING STREAMLINE

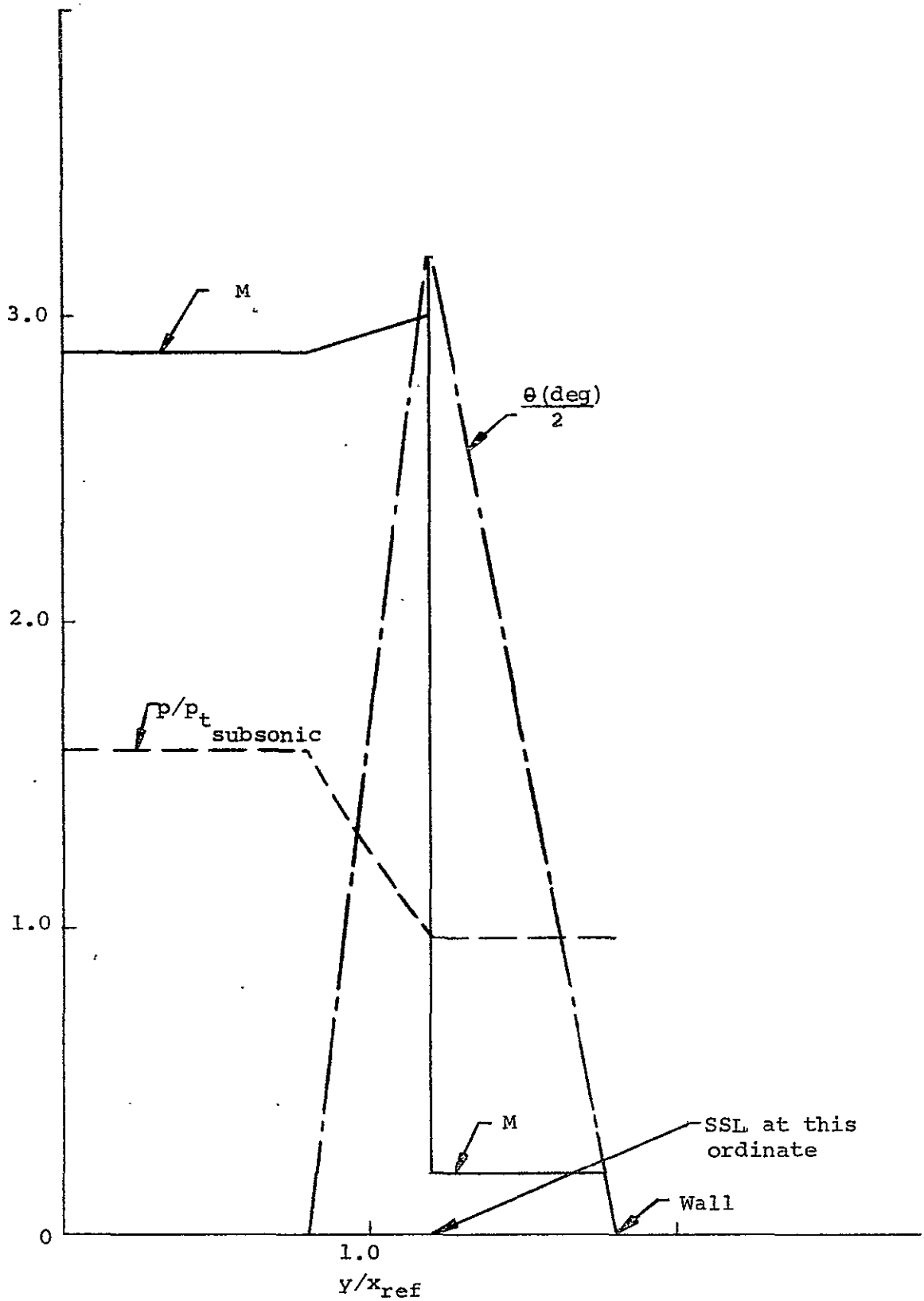

FIGURE 11 - PROFILES OF PRESSURE, MACH NUMBER, AND FLOW ANGLE AT INITIAL STATION

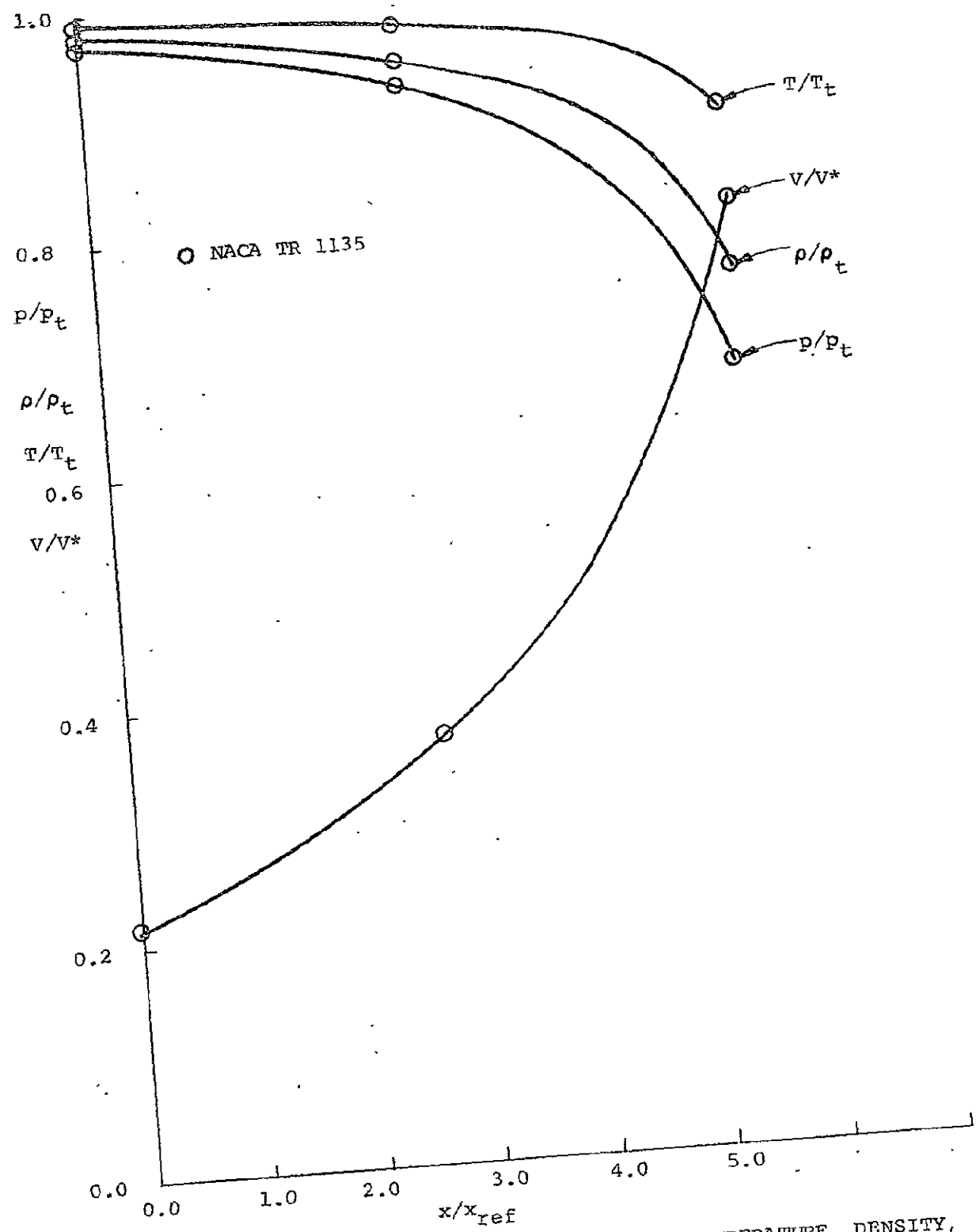

FIGURE 12 - AXIAL VARIATIONS IN PRESSURE, TEMPERATURE, DENSITY, AND VELOCITY FOR ONE DIMENSIONAL SUBSONIC REGION

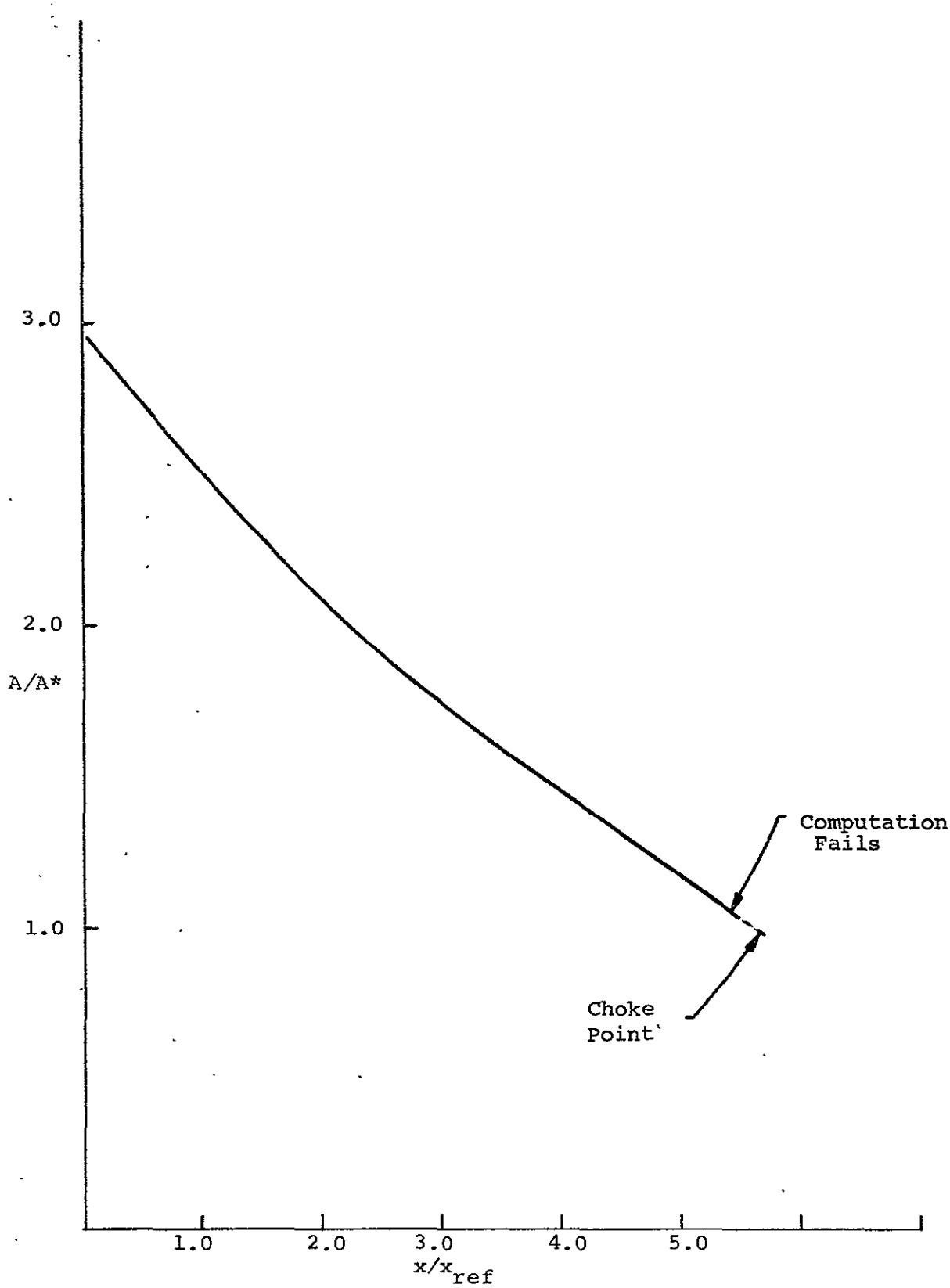

FIGURE 13 - COMPUTED AREA VARIATION OF SUBSONIC REGION

FIGURE 14

SCALE DRAWING OF CORNELL LAB. ETHYLENE-OXYGEN ROCKET ENGINE

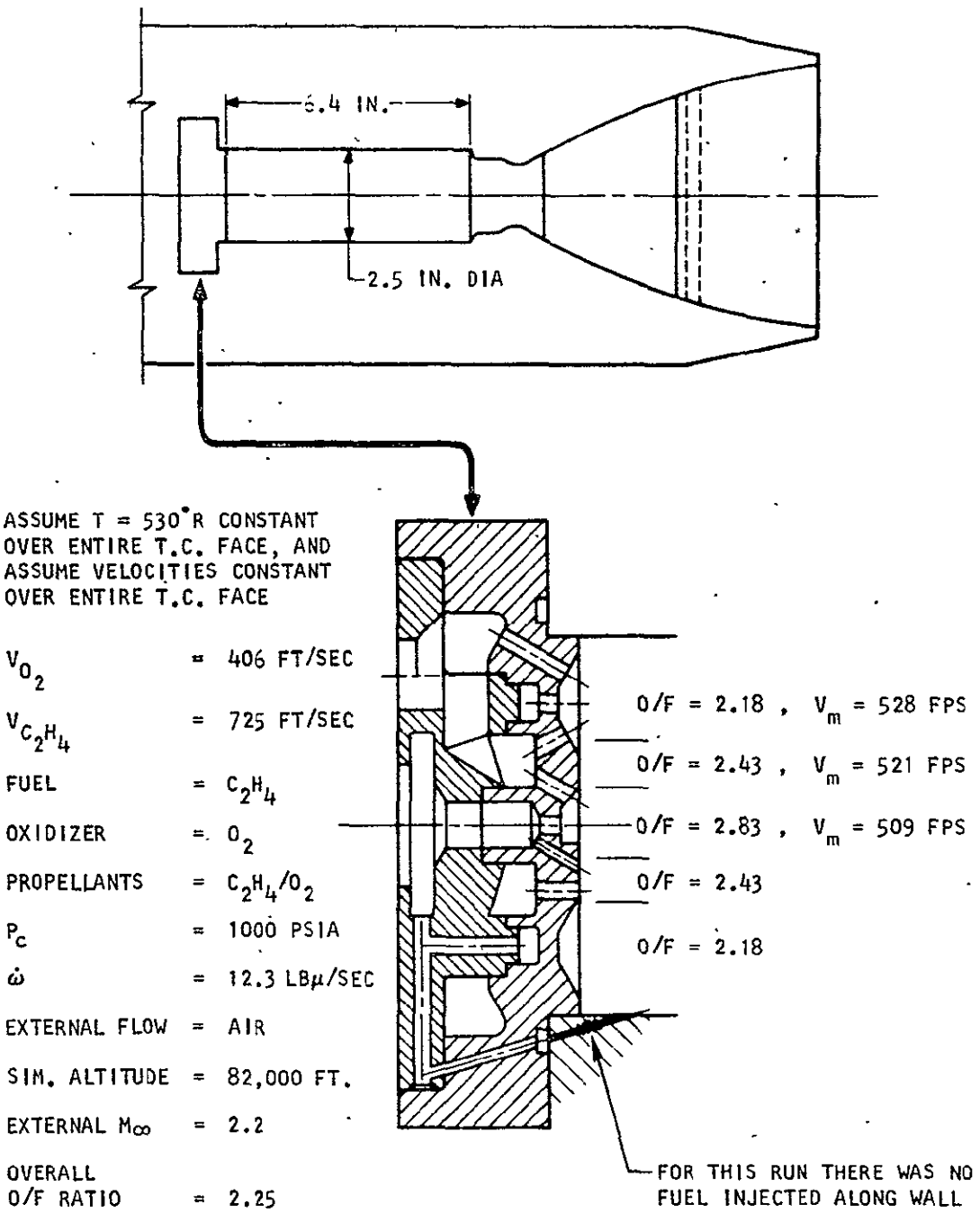

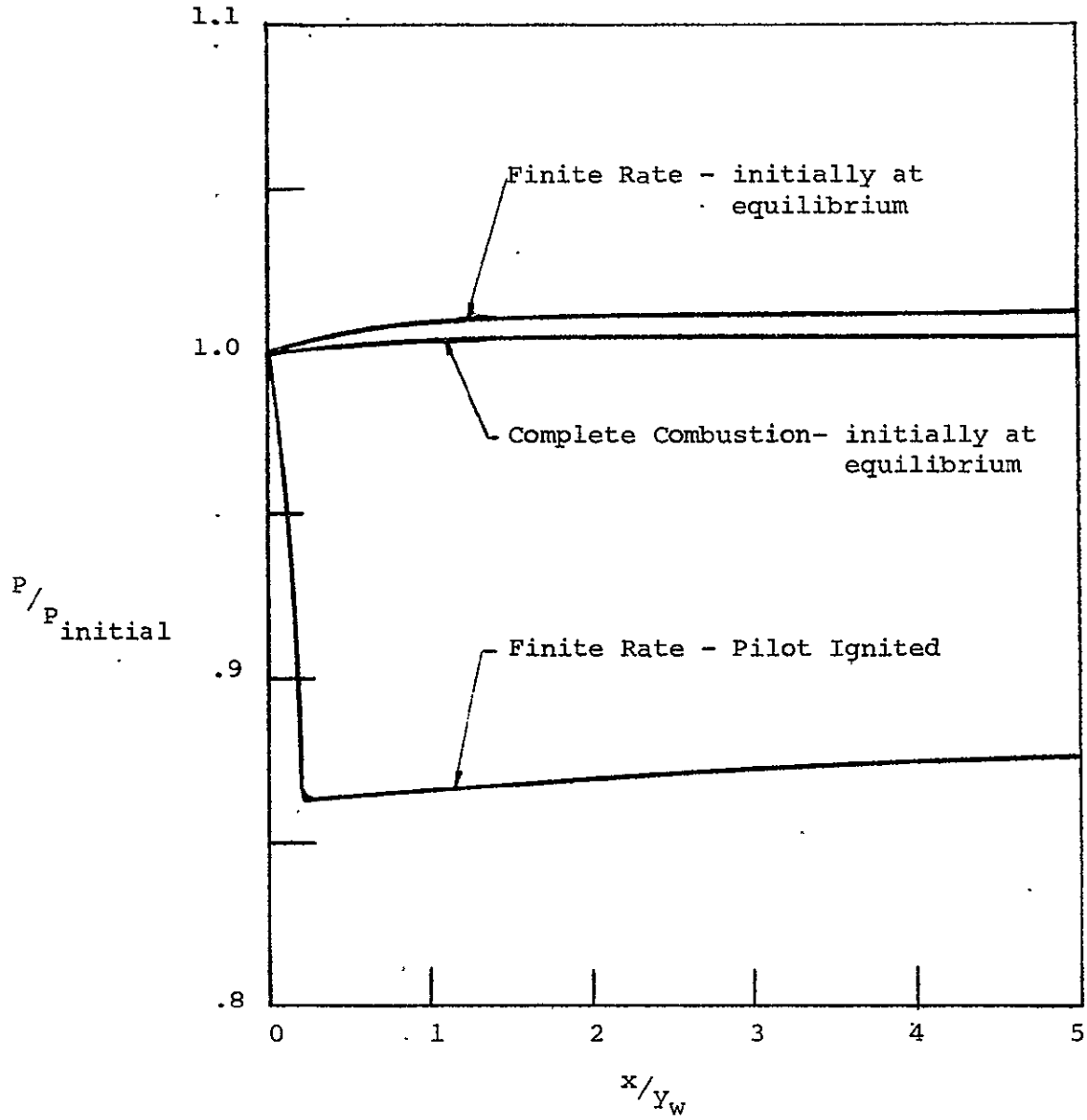

FIGURE 15 - AXIAL STATIC PRESSURE COMPARISON

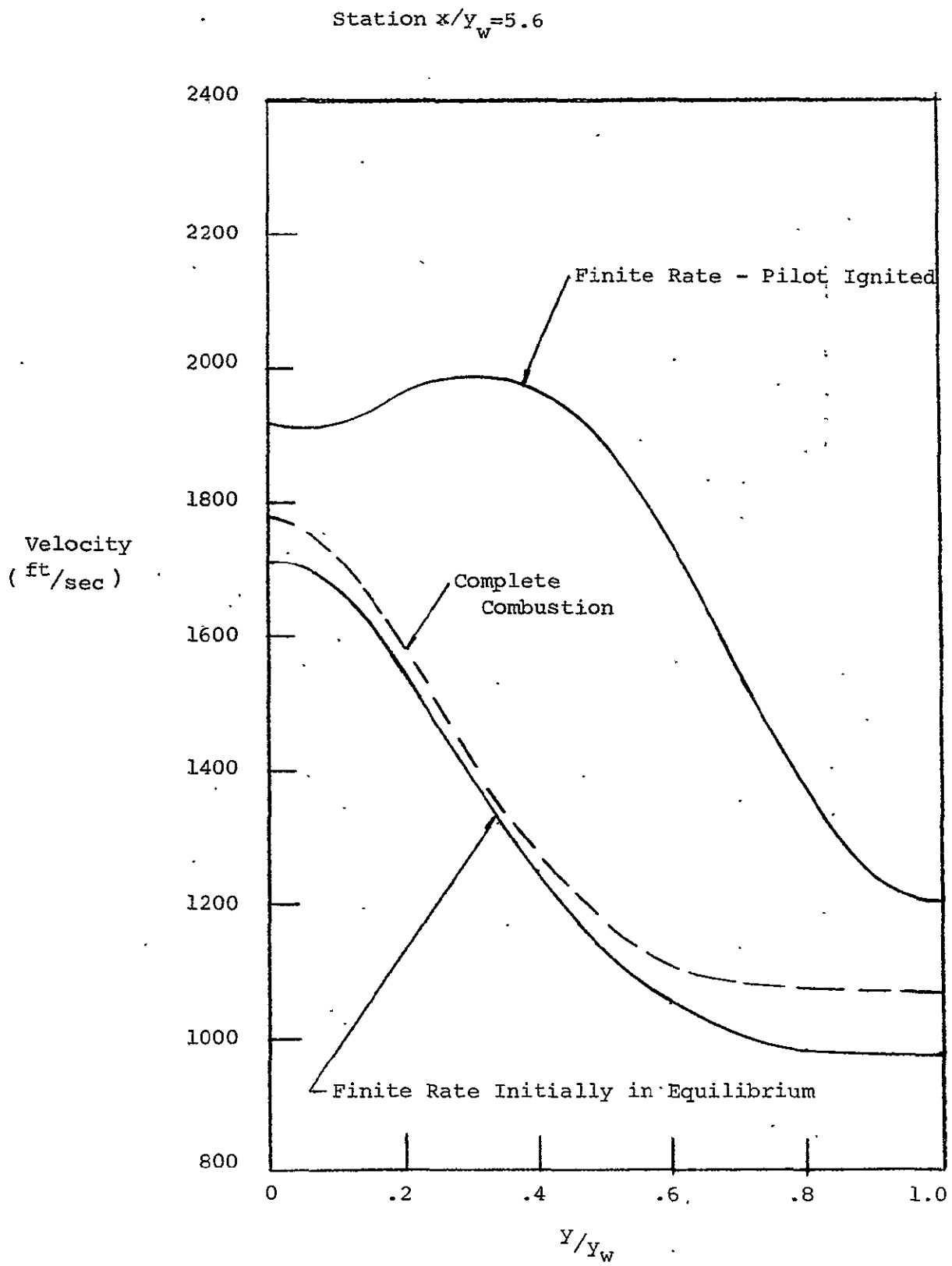

FIGURE 16- VELOCITY PROFILE COMPARISON

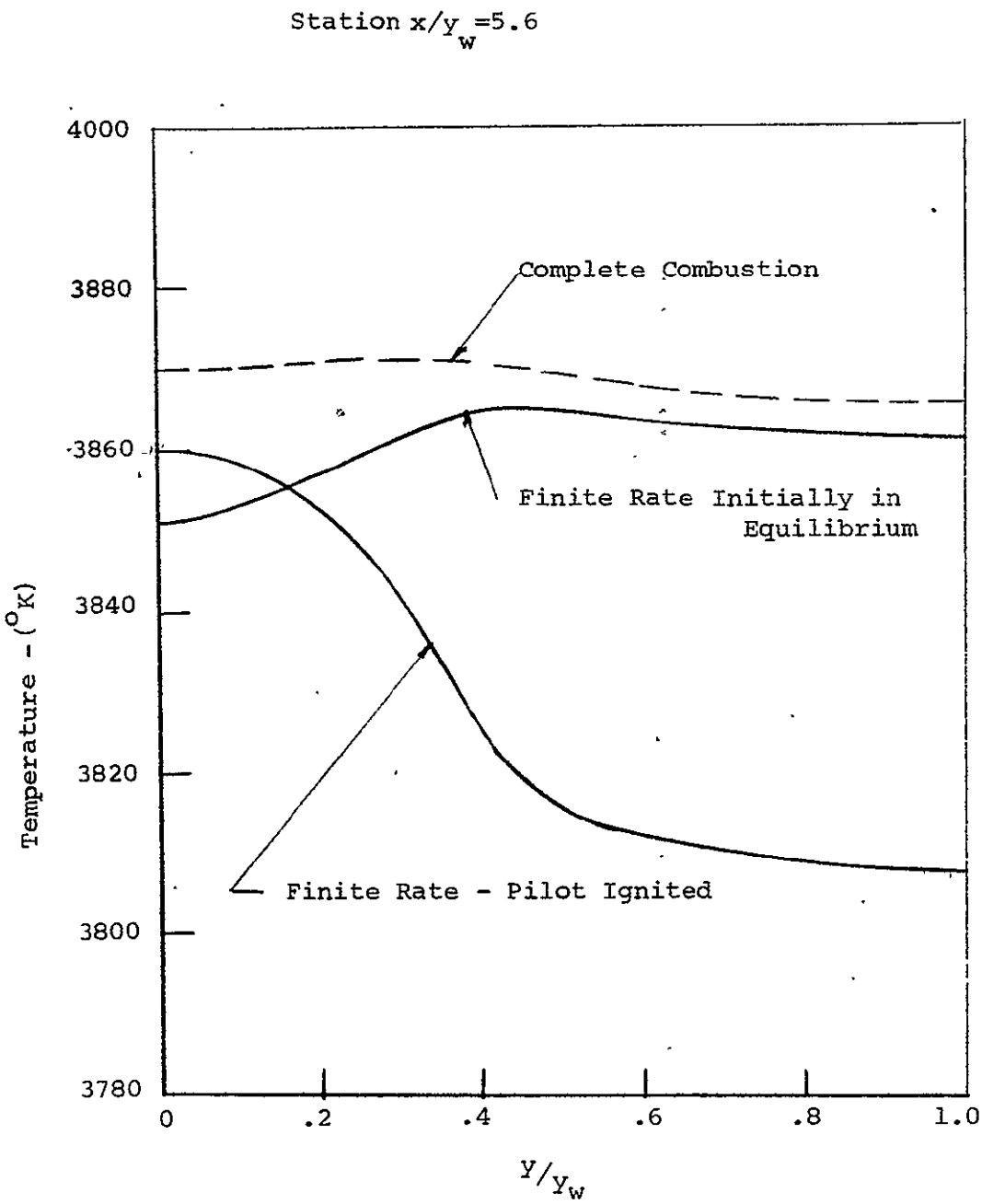

FIGURE 17 - TEMPERATURE PROFILE COMPARISON

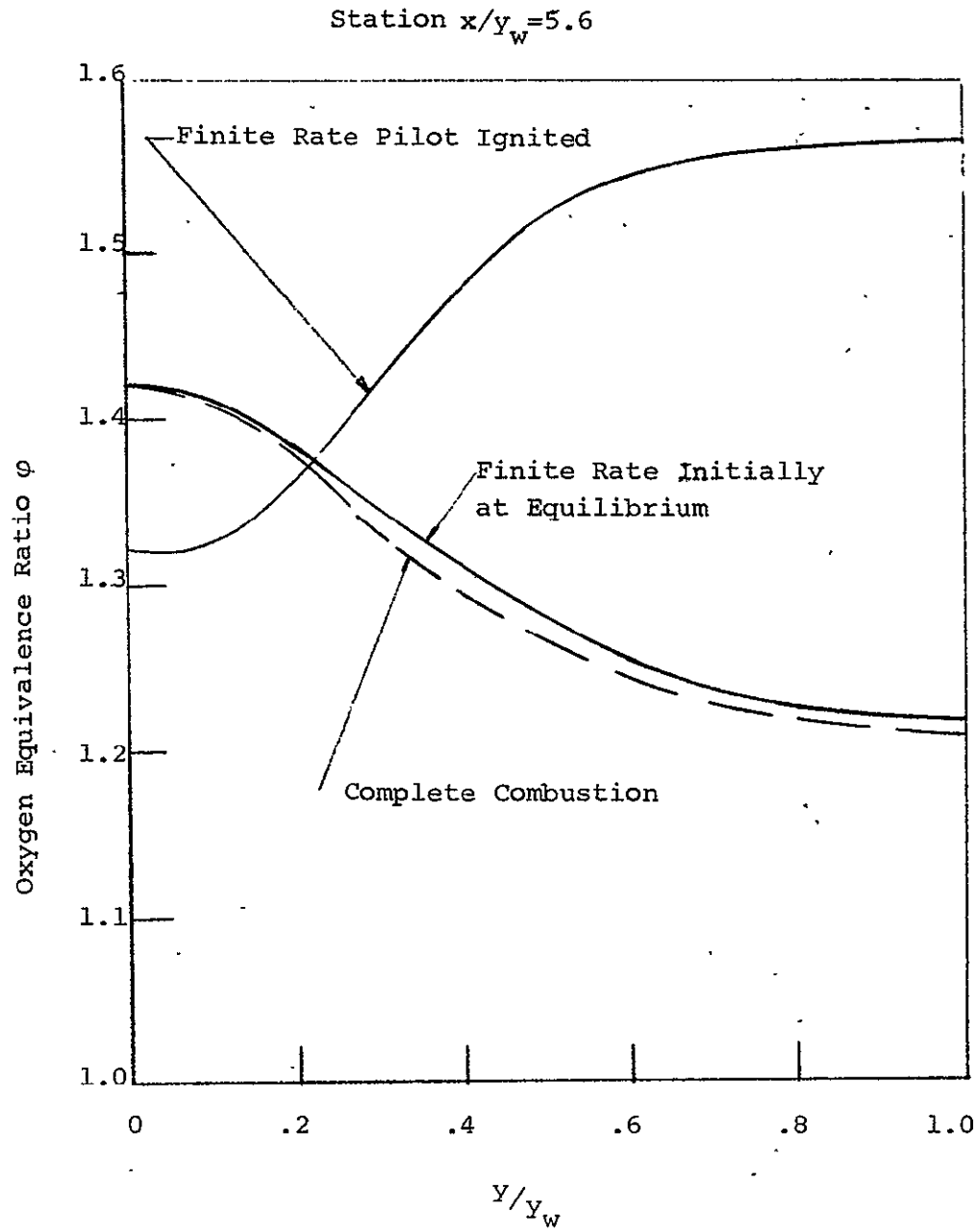

FIGURE 18- OXYGEN EQUIVALENCE RATIO PROFILE COMPARISON

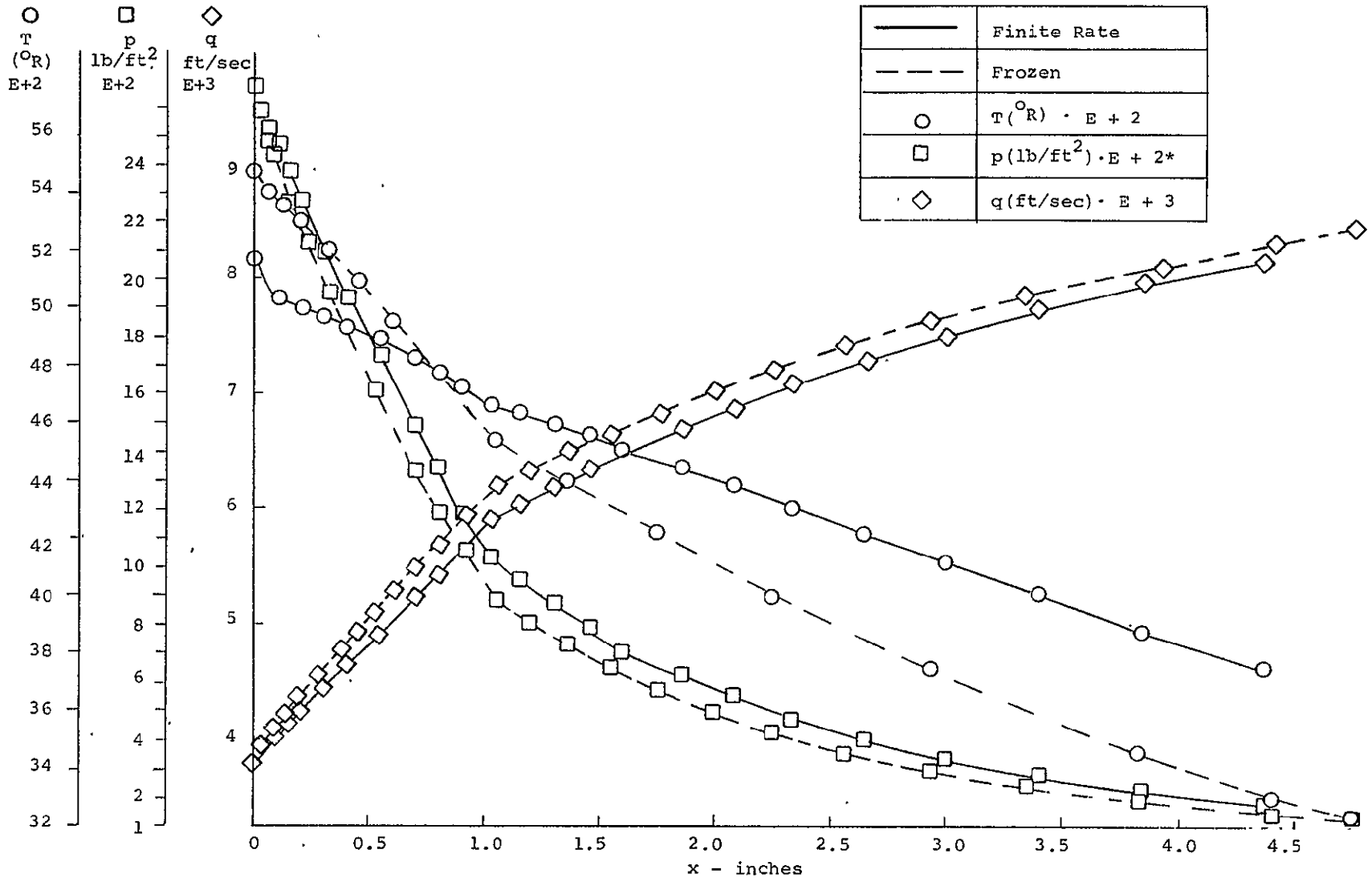

FIGURE 19a - WALL

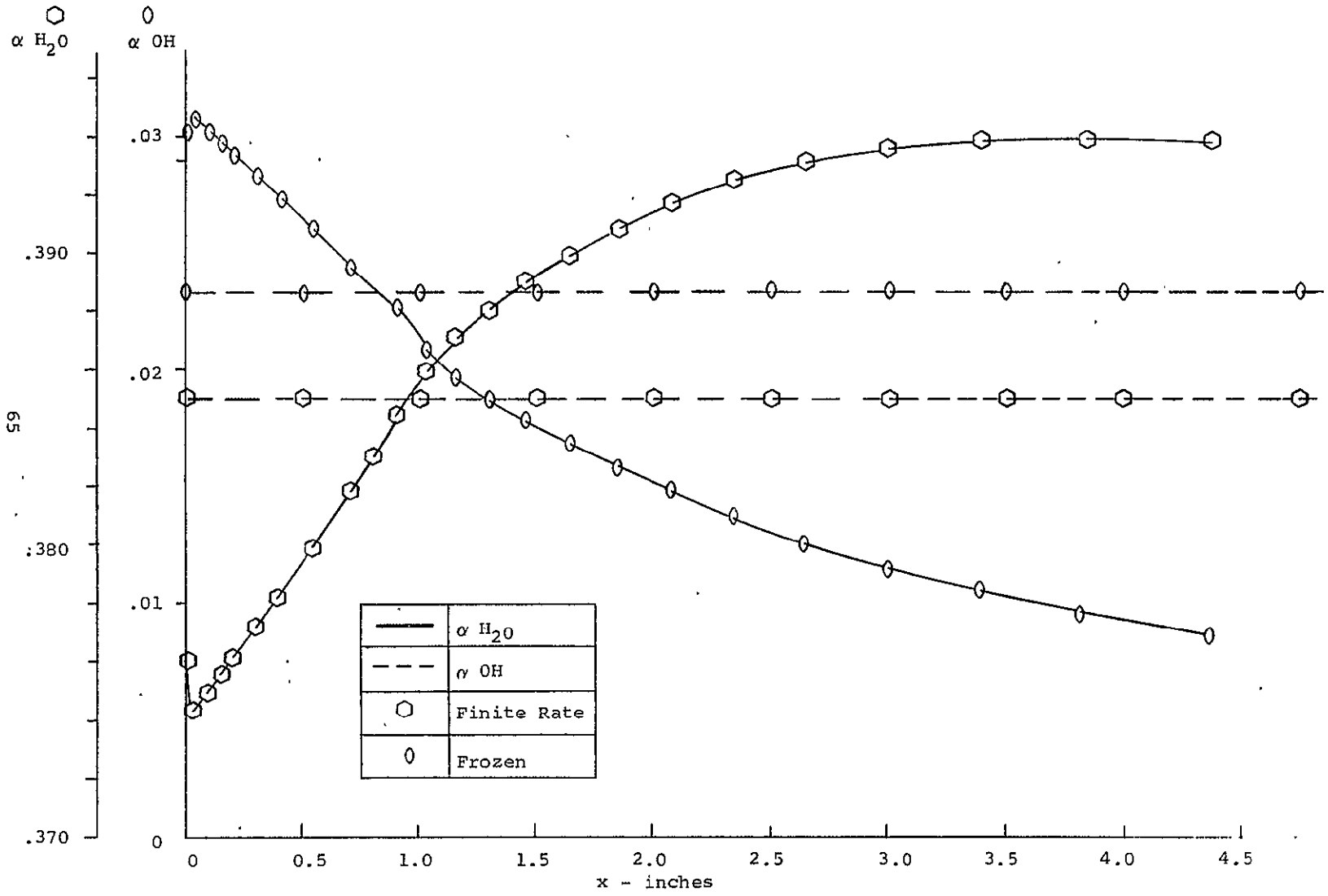

FIGURE 19b - WALL

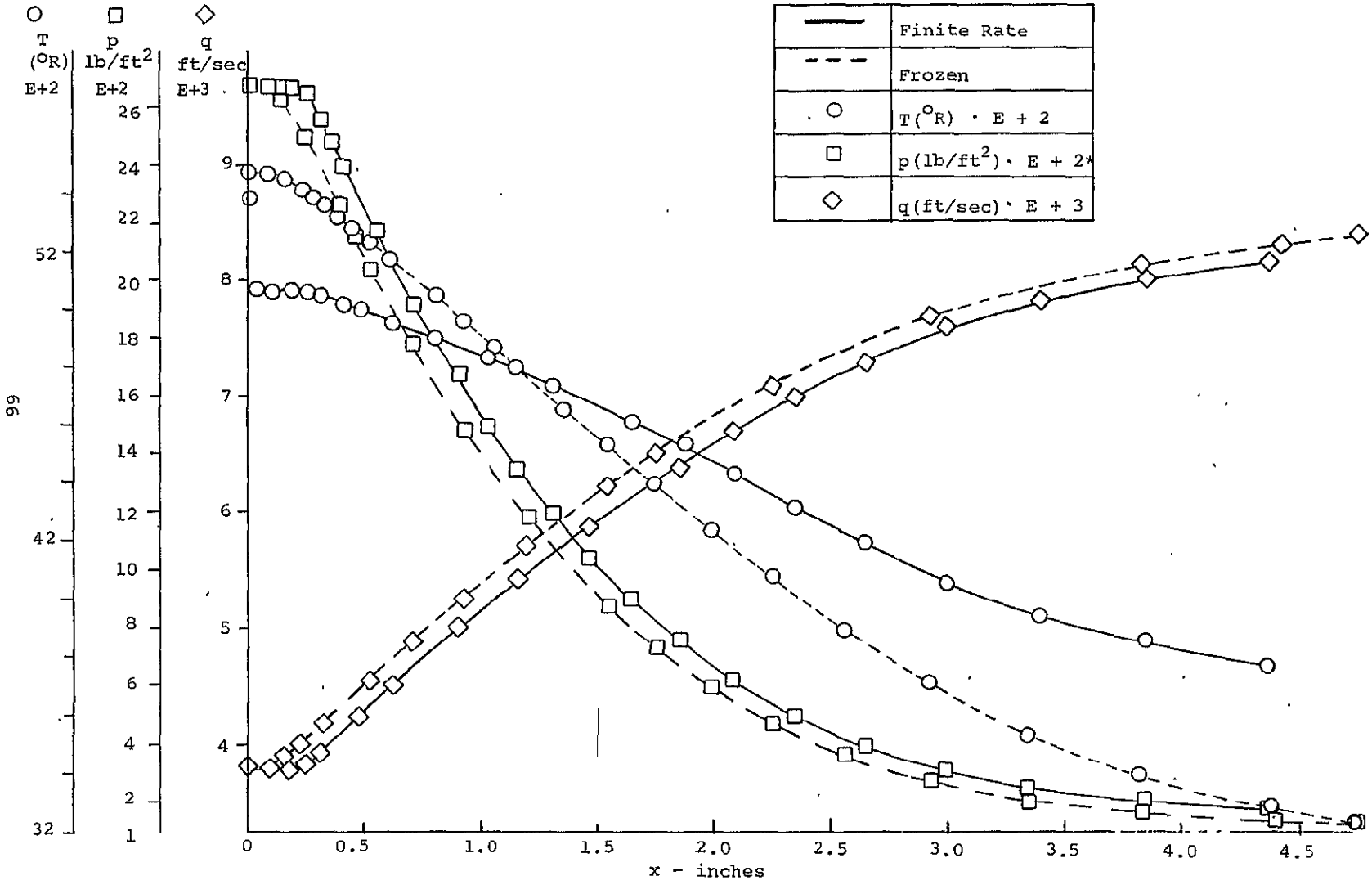

FIGURE 20a - CENTERLINE

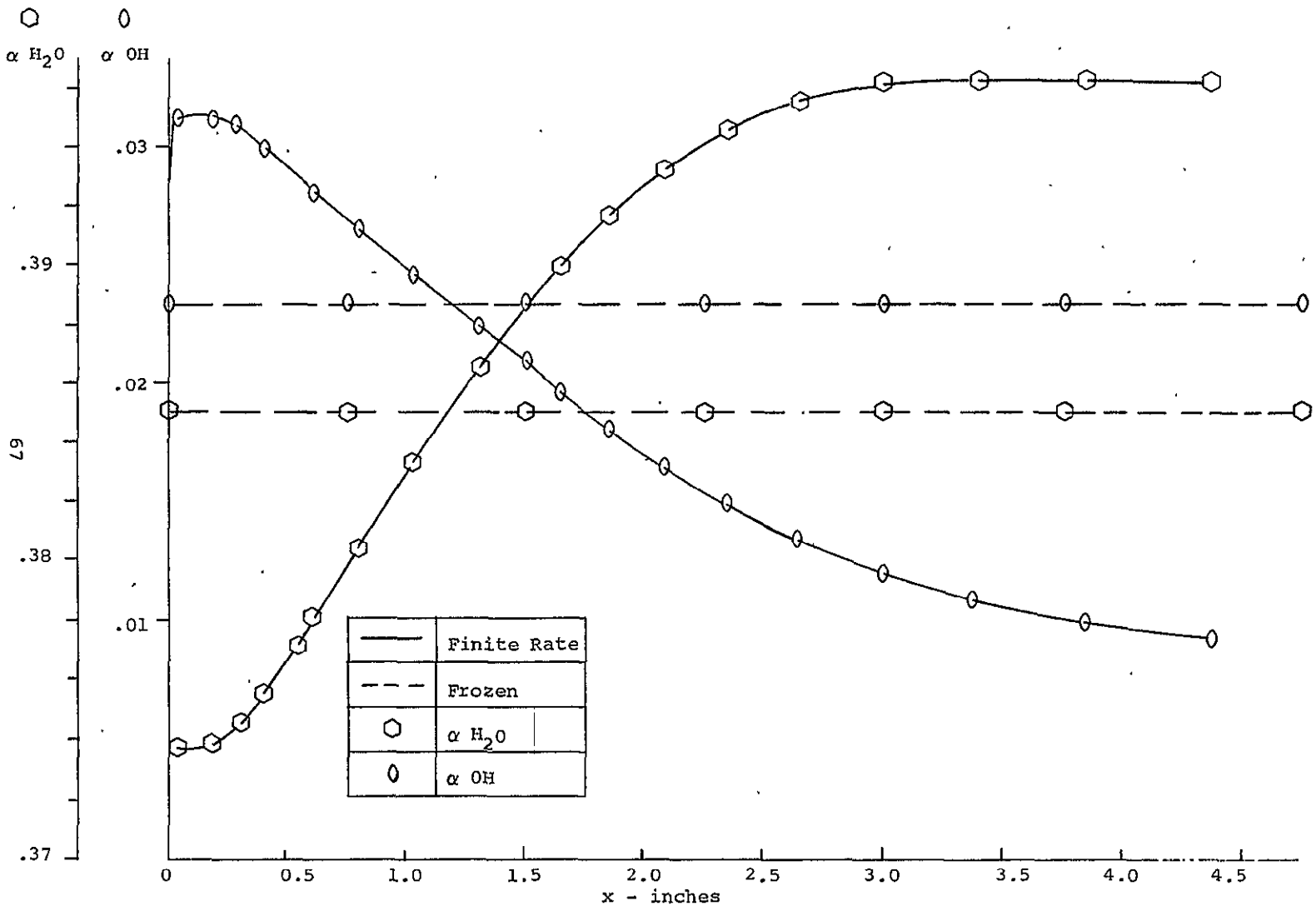

FIGURE 20b - CENTERLINE

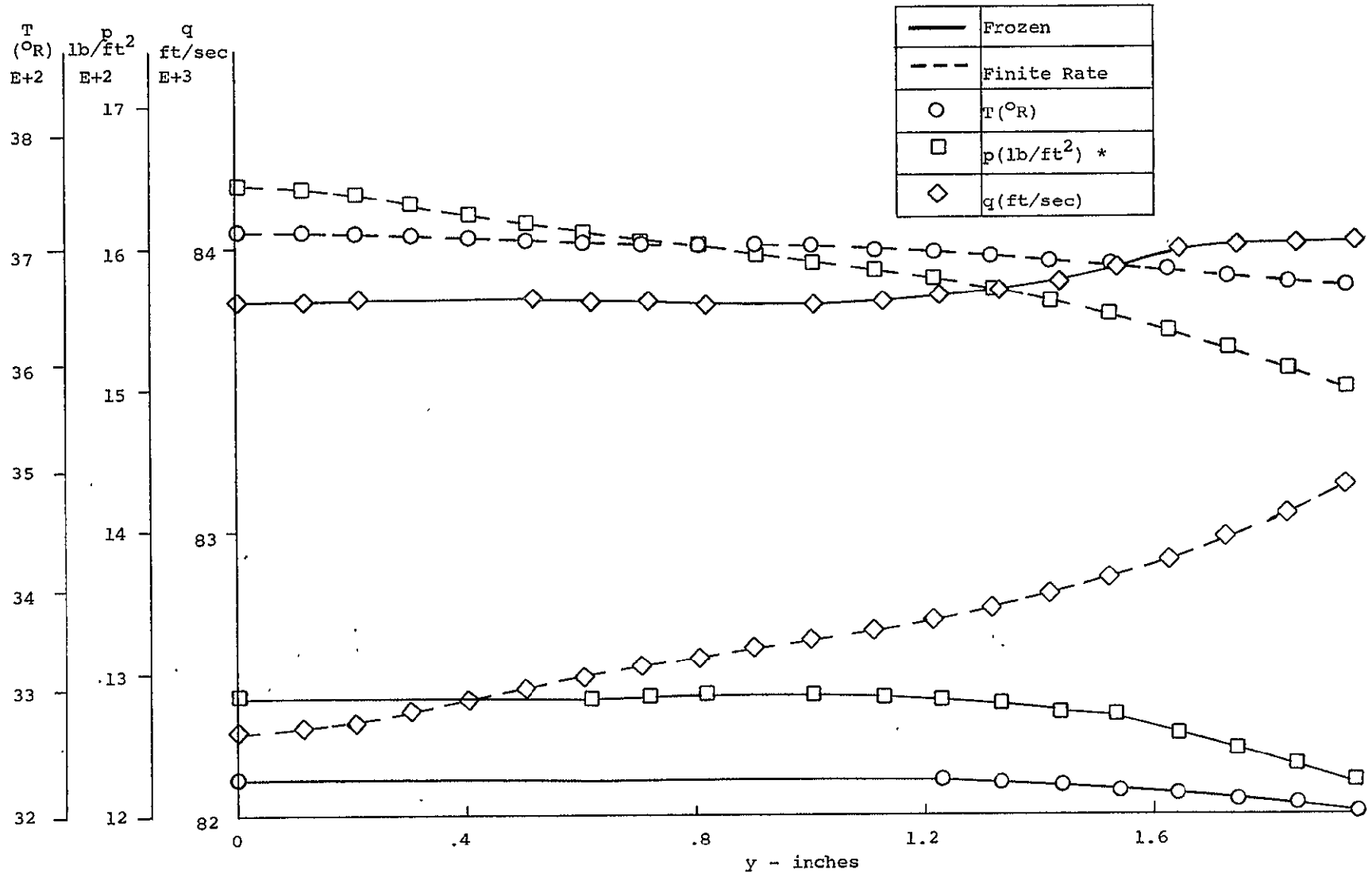

FIGURE 21 - END STATION